International Journal of Pharmaceutics 691 (2026) 126591

Contents lists available at ScienceDirect

International Journal of Pharmaceutics

journal homepage: www.elsevier.com/locate/ijpharm

Rosmarinic acid-eluting contact lenses as a multifunctional therapeutic system for diabetic ocular complications

Ana Centeno Duarte [a,d], Nadia Toffoletto [a,b,d,**], Rita Martins Pais [a,c], Zélia Lumack do Monte [c], Madalena Salema-Oom [d], Sandra Tenreiro [c], Ana Paula Serro [a,d,*]

[a] Centro de Química Estrutural (CQE), Chemical Engineering Department and Institute of Molecular Sciences, Instituto Superior Técnico, University of Lisbon, Av. Rovisco Pais 1, 1049-001 Lisbon, Portugal
[b] ADDRes Lab, Department of Food and Drug, University of Parma, Parco Area delle Scienze 27/A, 43124 Parma, Italy
[c] iNOVA4Health, NOVA Medical School, Campo Mártires da Pátria, 130, 1169-056 Lisbon, Portugal
[d] Egas Moniz Centre for Interdisciplinary Research (CiiEM), Egas Moniz School of Health & Science, Campus Universitário, Quinta da Granja, 2829-511 Monte de Caparica, Almada, Portugal

ARTICLE INFO

Keywords:
Rosmarinic acid
Therapeutic contact lenses
Hydrogels
Diabetic eye

ABSTRACT

Drug-eluting contact lenses (CLs) offer a promising approach to treat diabetic eye diseases. Compared to conventional treatments such as eye drops, CLs enhance drug bioavailability and residence time on the eye, while addressing patient compliance issues. Additionally, CLs are a safer alternative to ocular injections. In this study, CLs were designed for the sustained release of rosmarinic acid (RA), a natural polyphenol known for its antioxidant, anti-inflammatory, antibacterial and neuroprotective properties, which has been proposed as an alternative therapy for diabetic ocular complications. Acrylic and silicone-based hydrogels were produced and pre-treated with vitamin E. A sustained release of RA for up to 24 h was achieved under hydrodynamic conditions, which is compatible with the use of this hydrogel as daily CLs. Comprehensive characterization confirmed that the hydrogel's physicochemical properties met commercial CLs standards, while no signs of ocular irritation nor cytotoxicity were observed *in vitro*. *Ex vivo* studies demonstrated that the drug could permeate through ocular tissues. The ocular RA distribution after the CL application was estimated *in silico*. Finally, the neuroprotective effect of RA was evaluated *ex vivo* in porcine retinal explants, confirming the therapeutic relevance of the designed hydrogels in the treatment of the diabetic eye.

1. Introduction

Diabetes mellitus is one of the most concerning global health issues of the XXI century, affecting 536.6 million adults (20–79 years) in 2021, with numbers expected to increase to 783.2 million by 2045 (Sun et al., 2022). This disease affects the physiology and structure of the body's macro- and micro-vasculature, with the eyes being among the most vulnerable organs (Banday et al., 2020). Uncontrolled diabetes can lead to a variety of ophthalmologic diseases, including glaucoma, cataracts, diabetic macular oedema and diabetic retinopathy (Han et al., 2018; NIDDK, 2017), the latter being the most common diabetes-driven ocular complication and the major cause of blindness for individuals of working age (Kropp et al., 2023). These conditions arise from chronic hyperglycaemia, which affects a multitude of physiological processes, leading to alterations in the integrity of the vasculature, abnormal cell functioning and disruption of tissue homeostasis. At the core of these changes are oxidative stress, chronic inflammation, neurodegeneration, and uncontrolled neovascularisation.

Besides surgical intervention, the current standard treatment of the diabetic eye consists primarily of glycaemic control (Zhang et al., 2015), paired with various forms of drug administration to control the eye's intraocular pressure, prevent the abnormal growth of blood vessels and inhibit key pathological mechanisms (Kattar et al., 2021). Diseases of the posterior segment, like diabetic macular oedema and proliferative diabetic retinopathy (PDR), are generally treated with intravitreal injections of vascular endothelial growth factor (VEGF) inhibitors such as bevacizumab, ranibizumab and aflibercept (Tashima, 2024). VEGF antagonists have the potential to inhibit the abnormal growth of blood

* Corresponding author at: Centro de Química Estrutural, Instituto Superior Técnico, University of Lisbon, Av. Rovisco Pais, 1049-001 Lisbon, Portugal.
** Corresponding author at: ADDRes Lab, Department of Food and Drug, University of Parma, Parco Area delle Scienze 27/A, 43124 Parma, Italy.
E-mail addresses: nadia.toffoletto@unipr.it (N. Toffoletto), anapaula.serro@tecnico.ulisboa.pt (A.P. Serro).

https://doi.org/10.1016/j.ijpharm.2026.126591
Received 26 October 2025; Received in revised form 10 January 2026; Accepted 11 January 2026
Available online 12 January 2026

vessels by suppressing pathological angiogenesis and reducing vascular permeability, thus potentially preventing further vision loss and even improving it (Simó et al., 2014). While effective, these injections are invasive, and, as diabetes is a chronic disease, the repetition of such procedure can lead to a lack of patient compliance, as well as a plethora of serious side effects (endophthalmitis, retinal detachment, traumatic cataract, etc.) (Shikari et al., 2014). As chronic inflammation plays a crucial role in the progression of diabetic-related ocular complications, the administration of corticosteroids, such as triamcinolone acetonide, dexamethasone and fluocinolone acetonide, that not only modulate inflammatory mediators, but also have the potential to improve vascular leakage and abnormal growth, is commonly suggested (Chawan-Saad et al., 2019; Silva et al., 2009). Notwithstanding, steroidal drugs have been reported to have some associated risks, as they may increase ocular pressure and worsen the onset of cataracts (Carnahan et al., 2000; Storey et al., 2020). Consequently, these concerns have driven the interest in non-steroidal anti-inflammatory drugs (NSAIDs) such as bromfenac and nepafenac, which inhibit cyclooxygenase enzymes and decrease prostaglandin-mediated inflammation (Kim et al., 2010).

Due to the complex nature of diabetic eye complications, a synergistic treatment approach may be necessary. In the anterior segment, topical anti-inflammatory drugs (i.e. steroids, NSAIDs and immunosuppressors like cyclosporine A) have been shown to effectively control inflammation on the ocular surface as well as promote re-epithelialization (Han et al., 2018). Neuroprotective agents, on the other hand, have been found to be relevant in the preservation of retinal function by enhancing neuronal survival pathways (Zafar et al., 2019). Given the substantial role of oxidative stress in diabetic retinal damage and cataracts, antioxidant therapies such as carotenoids, pyruvate, vitamins C and E have also been explored as a promising strategy to ultimately improve the outcome of diabetic-related ocular complications (Pollreisz et al., 2010; da Silva et al., 2010; Wu et al., 2014).

Rosmarinic acid (RA), a natural polyphenol, has been previously studied in a diabetic context and has been shown to aid in the regulation of hyperglycemia by enhancing insulin sensitivity (Govindaraj et al., 2015; Inui et al., 2016). A RA-based approach may benefit from the drug's versatile action and ability to target multiple pathological mechanisms simultaneously (Fallarini et al., 2009; Khojasteh et al., 2020; Luo et al., 2020). For instance, in the posterior segment, RA has been shown to reduce vessel activity, thus potentially reducing retinal neovascularisation, which is related to diseases such as PDR and diabetic macular oedema (Kim et al., 2009; Vieira et al., 2020). Furthermore, previous research has identified RA as a promising candidate for delaying the onset of cataract and reducing its severity by interfering with cataract-associated proteins (Chemerovski-Glikman et al., 2018). Due to its structure, RA also has potent antioxidant properties relevant to counteracting oxidative stress in the anterior and posterior segments. It can stimulate the body's natural defences and effectively scavenge ROS and products of lipid and protein peroxidation (Chen et al., 2017; Mushtaq et al., 2015; Tsai et al., 2019). Additionally, RA helps control chronic inflammation in diabetic ocular complications by reducing pro-inflammatory cytokines and inhibiting major inflammatory pathways (El-Huneidi et al., 2023; Luo et al., 2020). Furthermore, RA is a promising candidate to mitigate retinal neurodegeneration by modulating important pathways and reducing neuronal cell apoptosis (Fachel et al., 2019).

Recent advancements in ocular drug delivery have explored various methods to effectively deliver RA to the eye. Drug delivery to the posterior segment of the eye faces significant physiological barriers that limit therapeutic efficacy, particularly when using topical formulations. The eye possesses highly efficient protective mechanisms, including rapid tear turnover, conjunctival and nasolacrimal drainage, and metabolic activity at the ocular surface, all of which markedly reduce drug residence time (Bachu et al., 2018). Moreover, the corneal epithelium and sclera restrict permeation, while the blood–retinal barrier tightly regulates the entry of circulating molecules into retinal tissues (Agrahari et al., 2016). These combined anatomical and physiological constraints result in extremely low drug bioavailability at the retina (Ramsay et al., 2023), making sustained and targeted delivery particularly challenging. Therefore, alternative strategies are being explored to overcome these limitations and improve therapeutic outcomes in retinal disease.

Vieira et al. developed biodegradable intravitreal implants to achieve a sustained delivery of RA to the posterior segment (Vieira et al., 2020). Nonetheless, this system faces some limitations, namely in terms of the procedure's invasiveness and potential complications. In turn, Silva et al. explored the use of chitosan nanoparticles to deliver RA through topical administration, having found that it improved mucoadhesion but not drug permeability (da Silva et al., 2016). In another study, RA-conjugated gelatin nanogels were developed and showcased excellent results for the treatment of dry eye disease. However, they specifically targeted the anterior segment and were not designed to treat the retina, where several diabetes-related ocular complications manifest (Zhou et al., 2024).

In this context, drug-eluting contact lenses (CLs) emerge as a promising alternative for the ocular delivery of RA through a user-friendly and non-invasive method, capable of treating both the anterior and posterior segments of the eye. Compared to intravitreal injections, which are invasive and associated to serious risks, and to traditional eye drops, which exhibit poor bioavailability due to rapid tear clearance, soft contact lenses (SCLs) not only increase patient autonomy and compliance to the treatment but also improve bioavailability by extending the drug's residence time on the cornea (Gause et al., 2016; Xu et al., 2018).

The present study aims to develop hydrogel-based SCLs able to deliver RA in a sustained manner to achieve therapeutically relevant concentrations in the ocular fluids/tissues for the treatment of the diabetic eye. Strategies were adopted to optimise the drugs' loading and release profiles. Then, hydrogels were characterised to ensure they met the functional, mechanical, chemical and biocompatibility standards for CLs. Additionally, ocular drug permeability and ocular drug distribution were determined to more accurately evaluate the efficacy of delivery of the drug-eluting CLs, while the therapeutic potential was assessed through antioxidant and neuroprotective assays.

2. Materials and methods

2.1. Materials

Rosmarinic acid (RA) (CAS 20283–92-5), N-vinyl pyrrolidone (NVP) (CAS 88–12-0), 2-Hydroxyethyl methacrylate (HEMA) (CAS 868–77-9), N-(3-aminopropyl) methacrylamide (APMA) (CAS 72607–53-5), ethylene glycol dimethacrylate (EGDMA) (CAS 97–90-5), azobisisobutyronitrile (AIBN) (CAS 78–67-1), sucrose (CAS 57–50-1), hydrochloric acid (HCl) (CAS 7647–01-0), sodium chloride (NaCl) (CAS 7647–14-5), isopropanol (CAS 67–63-0), dimethyl sulfoxide (DMSO) (CAS 67–68-5), 3-(4,5-Dimethylthiazol-2-Yl)-2,5-Diphenyltetrazolium Bromide (MTT) (CAS 298–93-1), trypan Blue solution (CAS 72–57-1), Triton™ X-100 (CAS 9036–19-5), penicillin–streptomycin stabilized solution (10,000 units of penicillin and 10 mg/mL of streptomycin), trypsin-EDTA solution, 4′,6-diamidino-2-phenylindole (DAPI) (CAS 28718–90-3) and phosphate-buffered saline (PBS) tablets were all purchased from Sigma-Aldrich (Darmstadt, Germany). Sodium hydroxide (NaOH) (CAS1310-73–2), octylphenoxypoly(ethyleneoxy)ethanol (IGEPAL®) (CAS 9002–93-1) and Mowiol® 4–88 (CAS 9002–89-5) were supplied by Merck (Darmstadt, Germany). 3-[tris(trimethylsiloxy)silyl]propylmethacrylate (TRIS) (CAS 17096–07-0) and 2,2-Diphenyl-1-picrylhydrazyl (DPPH) (CAS 1898–66-4) were purchased from TCI (Zwijndrecht, Belgium). Fetal bovine serum (FBS), DL-α-Tocopherol 97+% (Vitamin E) (CAS 10191–41-0), acrylic acid (CAS 79–10-7), optimal cutting temperature (OCT) compound, Gibco™ Antibiotic-Antimycotic solution (100X) (10000 units/mL of penicillin, 10000 μg/mL of streptomycin,

and 25 μg/mL of amphotericin B), Dulbecco's Modified Eagle Medium/ NutrientMixture F-12 (DMEM F12) and Alexa Fluor 488 donkey anti-rabbit were purchased from Thermo Fisher Scientific (Waltham, USA). Acetonitrile (CAS 75–05-8) was supplied by Chem-Lab (Zedelgem, Belgium). Distilled and deionised (DD) water (18 MΩcm, pH 6.7) was obtained from a Millipore system. Povidone-iodine (BETADINE®) (CAS 25655–41-8) was supplied from Viatris (Canonsburg, USA). Bovine Serum Albumin (BSA) (9048–46-8) was acquired from NZYTech (Lisbon, Portugal). Paraformaldehyde (PFA) (CAS 30525–89-4) was obtained from VWR®Chemicals BDH® (Radnor, Pennsylvania, USA). Brain-specific homeobox/ POU domain protein 3A (Brn3a) antibody (MAB1585) was purchased from Merk (Dallas, Texas, USA). Human primary corneal epithelial cells (ATCC PCS-700–010), corneal epithelial cell basal medium (ATCC PCS-700–030) and corneal epithelial cell growth kit (ATCC PCS-700–040) was purchased from LCG Standards (Barcelona, Spain). Hen's eggs were provided by Sociedade Agrícola da Quinta da Freiria (Roliça, Portugal). The porcine eyes were provided by SICASAL – Indústria e Comércio de Carnes (Gradil, Portugal) and CASO –Centro de Abate de Suínos do Oeste (Milharado, Portugal).

2.2. Drug characterization

2.2.1. Drug quantification

Drug quantification was carried out with a UV–Vis spectrophotometer (MultiskanGO, ThermoScientific, Porto Salvo, Portugal) throughout the full study, except for the *ex vivo* permeability test (section 3.6.2). RA's absorbance in PBS was read at 325 nm. Calibration curves were obtained in the range of 0.16–40 μg/mL.

For the *ex vivo* permeability assay, drug quantification was performed with a Waters Alliance 2695 Separations Module HPLC System equipped with a 996 Photodiode Array Detector (Waters Corporation, Milford, USA) and an Avantor® ACE® C18 column (particle size 5 μm, 25 cm x 4.6 mm). RA was detected at 325 nm with a retention time of 4.17 min. The mobile phase consisted of 0.1% acetic acid (pH 3) and acetonitrile in a 75:25 ratio. The analysis was performed at a flow rate of 1 mL/min with a 50 μL injection volume. Two calibration curves were prepared: a) in PBS to quantify the drug concentration during the permeability test, and b) in the extraction mixture (65% acetonitrile in water) to quantify the drug extracted from the ocular tissues. Both calibration curves were obtained within the 1.5–50 μg/mL concentration range.

2.2.2. Stability test

The drug's degradation profile over time (0, 3, 6, 24, 48, 120, 144 and 168 h) was assessed by evaluating the variation in UV–Vis absorption spectrum of an RA solution (400 μg/mL, prepared in PBS) under different conditions: (i) room temperature (RT) with the presence of light; (ii) RT in the absence of light; (iii) 36 °C with the presence of light; (iv) 36 °C in the absence of light; and (v) 4 °C in the absence of light.

2.3. Hydrogels production

2.3.1. Molecular interaction analysis

A preliminary screening was performed with AutoDock Tools 1.5.6 (MGL Tools, Scripps Research, La Jolla, CA, USA) to identify the monomers to include in the formulation of the RA-eluting hydrogels that enhance the material's affinity with the drug (Pereira-da-Mota et al., 2021). The 3D chemical structures of the monomers and of the drug were downloaded from the PubChem database (Kim et al., 2016) and files were converted with OpenBabel GUI software (OpenEye Scientific, Santa Fe, NM, USA). A docking simulation was carried out for each monomer-drug pair. Briefly, the monomer was identified as the "ligand" and the drug as the "macromolecule". The two-molecule interaction analysis was performed through the Lamarckian genetic algorithm. All torsions were allowed to rotate during docking. The value of the interaction's free energy (E) and dissociation constant (K_d) were obtained.

2.3.2. Hydrogel synthesis

Two types of hydrogels were prepared: acrylic and silicone-based, with a backbone polymeric network of HEMA and HEMA-NVP-TRIS, respectively. Based on prior molecular interaction analysis, increasing concentrations of the functional monomer APMA (0, 25, 50 and 100 mM) were included in the pre-polymeric mixture. The composition of the eight hydrogels is displayed in Table 1. AIBN was used as initiator and EGDMA as crosslinker.

First, the pre-polymeric mixtures were stirred at room temperature until complete solubilization of the monomers. No external solvent was added. Then, the mixtures were injected into moulds made of two pre-silanized glass flat plates separated by 0.5 mm-thick Teflon strips. The glass silanization followed a previously established protocol (Vazquez et al., 2006). The hydrogels were then obtained through bulk thermal polymerisation (60 °C, 24 h). Afterwards, the hydrogels were removed from the moulds and washed by soaking in DD water for a total of 5 days, with daily water renovation. The absorbance of the washing solutions was monitored daily by UV–vis spectrometry until no unreacted monomers could be detected (baseline returned to that of pure DD water, Supplementary Fig. S1). Finally, the hydrogel sheets were cut into 12 mm diameter discs (unless otherwise stated) and dried overnight in an oven at 40 °C prior to storage. Dry discs weighted approximately 12 mg.

2.4. Drug loading and release

2.4.1. Drug loading

Drug loading was performed by soaking the dry hydrogel discs (n = 3) in 1 mL of 2 mg/mL RA solution in PBS, at 4 °C for 72 h.

Vitamin E (VitE) pre-treatment was used as a strategy to improve the drug release kinetics from TRIS-hydrogels (Hsu et al., 2015). Briefly, prior to drug loading, the dry hydrogels were soaked for 24 h in a VitE-ethanol solution (3 mL) at concentrations of either 0.05 g/mL (TRIS-VitE1) or 0.1 g/mL (TRIS-VitE2). Then, the samples were submerged in DD water for 24 h to remove ethanol and dried overnight in an oven at 40 °C before being subjected to RA loading, as previously described.

To assess the drug amount loaded, the absorbance of the loading solution was measured before and after the loading process. The amount of RA loaded onto the hydrogels was calculated from the difference in RA concentrations between the two measurements (Toffoletto et al., 2024).

2.4.2. In vitro drug release

To obtain the *in vitro* release profile of RA, the loaded hydrogel discs (n = 3) were rinsed in PBS, blotted on absorbent paper to remove the drug excess from their surface and submerged in individual tubes containing 3 mL of PBS. Sink conditions were ensured. Samples were then placed on a shaker at 180 rpm and 36 °C. The release assays lasted 24 h: the first 12 h were conducted under controlled light exposure; thereafter the experiment proceeded in the absence of light. This simulates the daily use of contact lenses. At pre-defined times (1, 2, 3, 4, 5, 6, 7, 8 and 24 h), 0.3 mL aliquots of the release solution were collected for drug

Table 1
Composition of the eight hydrogels synthesized. Amounts of solids expressed in mass units and of liquids in volume units.

Hydrogel	*HEMA (mL)*	*TRIS (mL)*	*NVP (mL)*	*APMA (mg)*	*AIBN (mg)*	*EGDMA (μL)*
HEMA	*3.0*	0	0	*0*	*15*	*17*
HEMA25	*3.0*	0	0	*13.5*	*15*	*17*
HEMA50	*3.0*	0	0	*27.0*	*15*	*17*
HEMA100	*3.0*	0	0	*54.0*	*15*	*17*
TRIS	*0.65*	*1.1*	*1.25*	*0*	*15*	*17*
TRIS25	*0.65*	*1.1*	*1.25*	*13.5*	*15*	*17*
TRIS50	*0.65*	*1.1*	*1.25*	*27.0*	*15*	*17*
TRIS100	*0.65*	*1.1*	*1.25*	*54.0*	*15*	*17*

quantification and renewed with fresh PBS. The drug was quantified by UV–Vis spectrophotometry as described in section 2.2.1.

2.5. Physicochemical characterisation of the hydrogels

Based on the *in vitro* release profiles (section 3.3.1), TRIS-VITE1 was selected as the most promising hydrogel for the daily sustained release of RA. Thus, it was subjected to further characterisation. TRIS hydrogel was used as a control to evaluate the effect of VitE on the material's properties.

The surface wettability of the hydrogels was evaluated using a goniometer by the captive bubble method. The samples (n = 2) were hydrated in DD water, placed in a support and immersed in a quartz liquid cell filled with water. A micrometric syringe with a curved needle was used to form and place air bubbles under the material. A video camera (JAI CV-A50, Novaut, Álava, Spain) attached to an optical microscope (Wild M3Z, Leica Microsystems, Germany) was used to capture images. A total of 8 bubbles was produced for each sample. The images were analysed using the ADSA software (Applied Surface Thermodynamics Research Associates, Canada).

The impact of VitE pre-treatment on the chemical structure of the hydrogel TRIS was assessed through Attenuated Total Reflectance Fourier Transform Infrared (ATR-FTIR) spectroscopy using a spectrometer Spectrum Two FT-IR from PerkinElmer® (Waltham, MA, USA), in the wavenumbers range 400–4000 cm^{-1}. The hydrogels (TRIS and TRIS-VitE1) were dried for 24 h at 40 °C before the analysis. VitE was also tested for comparison. During the analysis, the samples made contact with the diamond crystal ATR accessory (PerkinElmer®, Waltham, MA, USA). The spectra were recorded with a resolution of 1 cm^{-1} and normalised using Prism 9.5.1 software (GraphPad, San Diego, CA, USA).

Hydrogel's surface morphology was assessed with a scanning electron microscope (SEM) (S-2400, Hitachi, Japan). The samples were previously lyophilized overnight at −60 °C and 0.025 mbar, and coated in a gold/palladium film with a Quorum Technologies sputter coater. The SEM images of the hydrogels' surface were acquired at 3500x magnification.

The tensile behaviour of the hydrogels was studied using a TA.XT Express Texture Analyser (Stable Micro Systems, Godalming, UK). The samples were cut into a dog-bone shape (2.5 mm width and ≈ 0.5 mm thickness, n = 4). Testing was conducted at 0.5 mm/s up to failure, with a trigger force of 0.005 N. The Young's modulus (E) was determined as the slope of the stress–strain curve in the 5–20% strain range (Vivero-Lopez et al., 2021).

As RA may affect the light transmittance of the hydrogels, loaded samples (n = 3) were characterized regarding this property. Measurements were done using a UV–Vis spectrophotometer in the range 200 to 800 nm, to ensure the material fulfilled the optical requirements to be used as CLs.

The equilibrium swelling ratio (ESR) of the hydrogels upon immersion in the drug solution was also determined. The hydrogel discs' (n = 3) were weighted prior to and after soaking, and ESR the was calculated using Equation (1), where W_h represents the final (hydrated) weight of the samples and W_d their initial (dry) weight.

$$ESR(\%) = \frac{W_h - W_d}{W_d} \times 100 \quad (1)$$

2.6. Biocompatibility study

2.6.1. Sterilization

Hydrated hydrogels were sterilised by autoclave (Uniclave 88, AJC, Portugal) at 121 °C for 20 min (Galante et al., 2018). Due to the thermal instability of VitE and RA, the VitE pre-treatment and drug loading were performed after the material's sterilisation and under sterile conditions (the used solutions were filtered using filters with 0.2 μm pores). The effect of sterilisation on the release profile and on the hydrogel's properties (in terms of chemical structure and mechanical properties) was assessed as described in Sections 2.4.2 and 2.5.

2.6.2. Cytotoxicity

Cell viability tests were conducted to (i) evaluate the potential cytotoxicity of the designed hydrogels and (ii) determine the minimum cytotoxic concentration of RA. The assays were conducted using human primary corneal epithelial cells (ATCC PCS-700–010), according to the ISO 10993–5:2009 standard (ISO 10993-5, 2009). Cells were cultured in corneal epithelial cell basal medium (ATCC PCS-700–030) enriched with corneal epithelial cell growth kit (ATCC PCS-700–040) and 1% penicillin–streptomycin, at 37 °C in a humidified environment with 5% CO_2.

The cytotoxicity of sterile TRIS-VitE1 hydrogels, either unloaded or loaded with RA, was evaluated by indirect contact (Meschini et al., 2020). First, cells were seeded in a 12-well plate ($9x10^4$ cells/well) and incubated for 24 h. Then, the hydrogel discs (n = 4, 8 mm diameter) were rinsed in PBS, blotted and placed in 12 mm diameter inserts (Transwell®, Corning, Glendale, AZ, USA). The inserts were then transferred onto the cell-seeded plate, with 500 μL of fresh medium on the bottom side and 200 μL on the apical side to reach a total of 700 μL/well. After an additional 24 h incubation, the inserts were removed from the plate and cells were rinsed with warm PBS before performing the MTT assay.

For the evaluation of the RA cytotoxic limit, cells were seeded in a 96-well plate ($1x10^4$ cells/well) and incubated for 24 h. Then, the medium was substituted with 100 μL of previously prepared RA dilutions (9.8–625 μg/mL in culture medium). After 24 h of incubation, cells were rinsed with warm PBS before performing the MTT assay.

Positive (cells + culture medium with 10% DMSO) and negative (cells + culture medium) controls were prepared.

For the MTT assay, 300 μL and 30 μL of MTT solution (10% MTT and 90% culture medium) were added to each well in the 12- and 96-well plates, respectively. The plates were incubated for 3 h. Afterwards, a formazan-dissolving solution (IGEPAL 0.1% in isopropanol with hydrochloric acid 4 mM) was added to the plates. The plates were placed overnight in a shaker at room temperature, protected from light. The absorbance was then measured at 565 nm in a microplate reader (Infinite 200 PRO, Tecan, Mannedorf, Switzerland). The obtained values were normalised to the negative control to quantify cell viability.

2.6.3. Ocular irritability test (HET-CAM)

The potential irritant effect of the hydrogels was estimated by the Hen's Egg test on the chorioallantoic membrane (HET-CAM) (ICCVAM, 2010; Wilson et al., 2015).

Fertilised hens' eggs (Sociedade Agrícola da Quinta da Freiria, SA, Portugal) were incubated for 9 days at 37 °C and 60% relative humidity. Then, the eggshell was cut above the air pocket and the inner membrane was hydrated with 0.9% NaCl. After 30 min of incubation, the inner membrane was removed, exposing the CAM. Sterile TRIS-VitE1 hydrogels (n = 3, 8 mm diameter), unloaded and loaded with the drug, as previously described (section 2.4.1), were placed on top of the CAM for 5 min. As positive and negative controls, 1 M NaOH and 0.9% NaCl were used, respectively.

The irritation score (IS) was assessed by observing the time of appearance (in seconds) of the following indicators: haemorrhages (t_h), lysis (t_l) and coagulation (t_c) (Equation (2)):

$$IS = \frac{(301 - t_h)}{300} \times 5 + \frac{(301 - t_l)}{300} \times 7 + \frac{(301 - t_c)}{300} \times 9 \quad (2)$$

According to the obtained value, the systems were classified as: non-irritating ($0 \leq IS \leq 0.9$); slightly irritating ($1 \leq IS \leq 4.9$); moderately irritating ($5 \leq IS \leq 8.9$); or severely irritating ($9 \leq IS \leq 21$).

2.7. Prediction of ocular drug distribution based on in vitro and ex vivo data

2.7.1. Hydrodynamic drug release

To better simulate the ocular environment, *in vitro* drug release was also performed under hydrodynamic conditions using a previously developed microfluidic cell (Pimenta et al., 2016). Briefly, RA-loaded TRIS-VitE1 hydrogel discs (n = 3, 12 mm diameter) were rinsed, blotted and placed within the inner chamber of the cell. The chamber was filled with 45 μL of PBS and incubated at 36°C. A constant flow rate of 3 μL/min was applied using a syringe pump (NE-1800 Eight Channel Programmable Syringe Pump, KF Technology, Rome, Italy) to simulate the tear renovation rate in a tolerant contact lens wearer (1.4–4.3 μL/min) (Glasson et al., 2006). At predetermined time points (1.5, 3, 4.5, 6, 7.5 and 24 h), aliquots of the release medium were collected from the exit port and drug concentration was determined by UV–Vis spectrophotometry (section 2.2.1).

2.7.2. Ex vivo permeability evaluation

An *ex vivo* permeability assay was conducted to determine the drug's ability to cross the cornea and sclera, and reach the internal tissues of the eye (Menduni et al., 2018). Freshly enucleated porcine eyes were collected from a local slaughterhouse (SICASAL – Indústria e Comércio de Carnes, S.A., Gradil, Portugal) and transported to the lab, immersed in PBS in an ice bath. The eyes were used within 3 h of animal death. Uniform portions of the cornea and sclera (n = 4) were isolated and clamped inside Franz diffusion cells (permeation area: 0.785 cm^2). A volume of 6.5 mL of PBS was added to the receptor chamber and 1 mL to the donor chamber. The Franz cells were placed in a thermostatic bath at 36°C with magnetic stirring of the receptor chamber, and allowed to equilibrate for 30 min. Then, the liquid in the donor chamber was replaced by 1 mL of 250 μg/mL RA solution in PBS, except for the control cells, where fresh PBS was left. The control was used to verify if any compounds that could interfere with the HPLC analysis were released from the tissues. At each time point (i.e., hourly up to 7 h), 1 mL aliquot was collected from the receptor chamber for drug quantification (section 2.2.1) and renewed with fresh PBS.

The cumulative amount of RA permeated, normalised by the permeation area, was plotted against time. The slope of the obtained linear regression represented the flux (J, in μg/cm^2s). The apparent permeability (P_{app}) was then calculated as follows, where $[RA]_0$ is the initial RA concentration in the donor chamber (Kim et al., 2021):

$$P_{app} = \frac{J}{[RA]_0} \tag{3}$$

The partition coefficient (K) of RA between the ocular tissues and PBS was calculated to estimate the potential for drug accumulation after administration. Briefly, samples of isolated tissues (cornea and sclera, n = 3, 10 mm diameter) were weighted and immersed in 1 mL of 250 μg/mL RA solution in PBS overnight. Then, the final concentration of the soaking solution ($C_{solution}$) was analysed by HPLC (section 2.2.1). Concurrently, the tissues were removed from the solution, blotted on absorbent paper and placed overnight in 1 mL of a solution of 65% acetonitrile in DD water for the extraction of the drug. The validation of this extraction method, performed by extraction of a known amount of drug from the tissues, is presented in the Supplementary Information (Fig. S2). After HPLC quantification, the drug extracted from the cornea and sclera was normalised by the weight of the tissues, obtaining the RA concentration in the tissue (C_{tissue}). The partition coefficient was calculated as follows:

$$K = \frac{C_{tissue}}{C_{solution}} \tag{4}$$

2.7.3. Modelling ocular drug distribution

Distribution of the RA eluted from the TRIS-VitE1 hydrogels in the various ocular parts was predicted using a previously validated physiology-based mathematical model (Toffoletto et al., 2023). The computational model included one mass balance differential equation for each tissue. This enabled the estimation of RA's concentration in the tears, aqueous humour, sclera and choroid, retina and vitreous humour. The model's inputs included characteristics of the drug and of the hydrogel, and anatomical and physiological ocular features of an animal model.

The drug-specific input values used for the simulation are reported in Supplementary Information (Table S1). In particular, the *ex vivo* permeability data across the sclera and the partition coefficient of RA with this tissue, obtained experimentally as described in Section 2.7.2, were used. Other required input values (the permeability of the drug through the conjunctiva and the inner limiting membrane, the partition coefficient of RA with retina, and the drug bioavailability in the aqueous humour) were estimated from previous research involving other drugs considered similar to RA in terms of lipophilicity ($logD_{7.4}$ = -2.1) and molecular weight (360.3 g/mol) (ChemSpider, n.d.; Serrano et al., 2021).

The *in vitro* drug release rate (R) was also required as an input value. R was obtained as the derivative of the release curve f over time, while f was obtained by fitting the release data from the hydrodynamic release (section 3.7.1) to an exponential curve (Equation (5)):

$$f = M_{released} \times \left(1 - e^{-t/T}\right) \tag{5}$$

where $M_{released}$ is the total amount of RA released, and T is the time constant obtained by curve fitting.

2.8. Evaluation of the therapeutic efficacy

2.8.1. Antioxidant activity

The antioxidant potential of the RA-eluting system was assessed by examining its ability to scavenge the stabilised radical DPPH•. To do this, hydrogel discs (8 mm diameter, n = 3) of (i) unloaded TRIS, (ii) unloaded TRIS-VitE1 and (iii) RA-loaded TRIS-VitE1 were immersed in 3 mL PBS for 24 h at 36 °C under agitation (180 rpm). A fresh RA solution (50 μg/mL) was also prepared to be tested as a control. Then, dilutions of the obtained release solutions and of the fresh RA solution were prepared in the concentration range of 3–50 μg/mL.

DPPH was dissolved in 100% ethanol at a concentration of 0.1 mM. The solution was obtained by 30 min of magnetic stirring, followed by 30 min of sonication. A volume of 200 μL of each of the previously prepared dilutions was mixed with 800 μL of the DPPH solution and left for 30 min protected from light. Afterwards, the absorbance was read at 517 nm.

The scavenging effect of the samples was determined with the following equation (Biswas et al., 2010):

$$DPPH\ Scavenging\ Effect\ (\%) = \left(1 - \frac{A_s}{A_c}\right) \times 100 \tag{6}$$

where A_s denotes the absorbance of the sample, and A_c represents the absorbance of the control (800 μL DPPH solution + 200 μL PBS).

2.8.2. Ex vivo neuroprotective activity

An *ex vivo* assay using porcine eyes was conducted to assess RA's neuroprotective potential in the retina (Teixeira et al., 2024). Firstly, the explant's culture medium, consisting of Dulbecco's Modified Eagle Medium/Nutrient Mixture F-12 (DMEM F12) supplemented with 5% Fetal Bovine Serum (FBS) and 2% antibiotic–antimycotic solution (Penicillin/Streptomycin/Amphotericin B) was prepared and stored at 4 °C. RA was diluted in the medium to achieve different concentrations: 86 ng/mL and 400 ng/mL.

The retina, choroid, and sclera were isolated from fresh porcine eyes. The tissue samples were cut with a 6 mm biopsy punch and placed in 12 mm cell culture inserts (Millipore® PIHP01250, Merck KGaA, Germany)

within a 24-well plate, where they were rinsed with PBS. The explants (n = 3) were divided into two groups: day 0 (D0) samples as negative controls, and day 2 (D2) samples to evaluate the neuroprotective effects of RA on degenerating tissues.

The D0 samples were fixed in 4% paraformaldehyde (PFA). After 1 h, the samples were washed twice in PBS and dehydrated by immersion for 1 h in sequentially increasing concentrations of sucrose-PBS solutions (10%, 20% and 30%) (Dewan et al., 2016). After being left overnight in 30% sucrose, the tissues were embedded in an optimal cutting temperature (OCT) compound within cryosectioning moulds, frozen on dry ice, and stored at −20°C until cryosectioning.

The D2 samples were incubated at 37°C and 5% CO_2 in a 24-well plate containing the previously prepared explants culture media supplemented with RA. Control explants were incubated in the medium without RA. After 2 days, the samples were fixed, dehydrated, and cryopreserved as described above.

The samples were cryosectioned with a cryostat (Leica CM3050 S, Leica Biosystems, Germany), yielding 14 μm-thick sections of the retina-choroid-sclera complex, which were then mounted in adhesive slides and stored at −20°C until the immunofluorescence (IF) assay. For the IF assay, the slices were washed thrice in 0.25% PBS-Triton X (PBS-T) (15 min of immersion each) before a blocking solution (0.25% PBS-T with 1% Bovine Serum Albumin (BSA) and 3% Donkey Serum (DS) was applied for 1 h at RT. To evaluate the neuroprotective potential, the slides were incubated with anti-brain-specific homeobox/POU domain protein 3A (Brn3a; 1:200) diluted in 0.25% PBS-T. Brn3a is a specific marker for retinal ganglion cells (RGCs), enabling the quantification of RGC survival (Meng et al., 2024).

The following day, samples were thawed for 20 min, washed with 0.25% PBS-T, and incubated for 1 h at RT with the secondary antibody (Alexa Fluor 488 goat anti-rabbit) and 4′,6-diamidino-2-phenylindole (DAPI; 1:10000) diluted in 0.25% PBS-T.

Finally, Mowiol® 4–88 was applied on top of the slides to facilitate the placement of a coverslip, before being stored overnight at −20°C to allow proper adherence. The slides were then sealed with nail polish. The microscopic images of randomly selected regions of the samples were captured at 40x magnification using an Axio Imager 2 microscope (ZEISS, Oberkochen, Germany) equipped with an Axiocam 506 mono microscope camera (ZEISS, Oberkochen, Germany) and illuminated with a HXP 120 V lighting unit (Leistungselektronik Jena GmbH, Jena, Germany). The number of $Brn3a^+$ cells per millimetre of tissue (cells/mm) was manually quantified using the Fiji Software.

2.9. Statistical analysis

All quantitative data are presented as mean ± standard deviation. Statistical analysis was performed using GraphPad Prism 10.3.1 (GraphPad, San Diego, CA, USA). Variables' conformity to the normal distribution was examined through the Shapiro–Wilk test. For normally distributed data, unpaired *t*-test (between two groups) or one-way ANOVA (for three or more groups) followed by Tukey's multiple comparisons tests were conducted. Non-normally distributed data were analysed using either the Mann-Whitney or Kruskal-Wallis with Dunn's multiple comparisons test. The threshold for statistical differences was considered $p < 0.05$ (*), $p < 0.01$ (**), $p < 0.001$ (***) and $p < 0.0001$ (****) with a confidence level of 95%.

3. Results and discussion

3.1. Drug stability

A decrease in absorbance was observed in the UV–vis spectra of the RA solution over time, indicating degradation of the drug (Supplementary Fig. S3). Such degradation appeared exacerbated by increased temperature (*i.e.*, 36 °C) and, to a minor extent, by exposure to light. The stability of RA in solution was maintained for the longest period (*i.e.*, at least one week) when stored at 4 °C without light. Therefore, these conditions were selected for the drug loading process, namely, in the soaking of the hydrogels in the RA solution.

3.2. Hydrogels synthesis

The use of a computational tool to simulate the affinity of RA with a range of monomers helped in the selection of the most suitable components for the polymer's structure. The results obtained from the molecular docking are displayed in Table 2.

A more negative value of E indicates that the drug-monomer pair presents a stronger interaction (Du et al., 2016). Likewise, a low value of K_d, indicates that the pairing tends to form a complex rather than separating (Nambiar et al., 2022). Consequently, TRIS and APMA were considered, amongst the tested monomers, the components with the strongest interactions with RA. This led to the design of two classes of hydrogels: acrylic-based hydrogels and silicone-based hydrogels, which were enriched with increasing APMA concentrations (Table 1).

After polymerisation, yellow aggregates were visible in the matrix of the TRIS-based hydrogels with the highest concentration of APMA (*i.e.*, TRIS50 and TRIS100, Supplementary Fig. S4A), which were therefore discarded as potential CL materials. The other hydrogels (i.e., HEMA, HEMA25, HEMA50, HEMA100, TRIS and TRIS25) resulted macroscopically homogeneous and were further tested.

3.3. Drug release in static conditions

3.3.1. In vitro drug release

The release profile of RA from the designed hydrogels in static conditions is shown in Fig. 1. For the HEMA-based hydrogels (Fig. 1A), the introduction of increasing APMA concentrations resulted in a slight increase in the cumulative amounts of drug released. Also, the presence of APMA did not improve the release kinetics, which was characterised by an initial burst in the first 2 h of release, followed by a plateau. The release profiles expressed in percentage of the drug released relatively to the total amount of drug loaded are reported in Supplementary Fig. S5Ai: 100% of the total amount loaded was released in the first 4 h, confirming the negligible effect of APMA on the release kinetics of RA in HEMA-based hydrogels.

TRIS hydrogels (Fig. 1B) released significantly higher amounts of RA compared to HEMA-based hydrogels and ensured a controlled release for 4 h, followed by a slower release over the subsequent hours. Nevertheless, the initial drug diffusion was still too rapid for the use of TRIS hydrogels as a daily drug-delivery platform. The addition of APMA (samples TRIS25) altered the release profile kinetics, resulting in a sustained release over 24 h. The improved kinetics of TRIS25 is clear when the release profiles are expressed as percentage of drug released (Supplementary Fig. S5Aii). Despite this improvement, the amount of drug released decreased significantly. Subsequently, to improve the

Table 2
Results of the molecular docking between each RA-monomer pairing in terms of interaction energy (E) and dissociation constant (Kd).

	E [Kcal/mol]	Kd [mM]
HEMA	−1.60	66.77
BEM	−1.58	68.92
APMA	−3.84	1.54
AAm	−1.94	37.96
AAc	−1.13	149.72
TRIS	−2.82	8.60
NVP	−1.96	36.54
MAA	−1.38	96.57

HEMA = Hydroxyethyl methacrylate, BEM = Butyl methacrylate, APMA = Aminopropyl methacrylamide, AAm = Acrylamide, AAc = Acrylic acid, TRIS = Tris(hydroxymethyl)aminomethane, NVP = N-vinylpyrrolidone, MAA = Methacrylic acid.

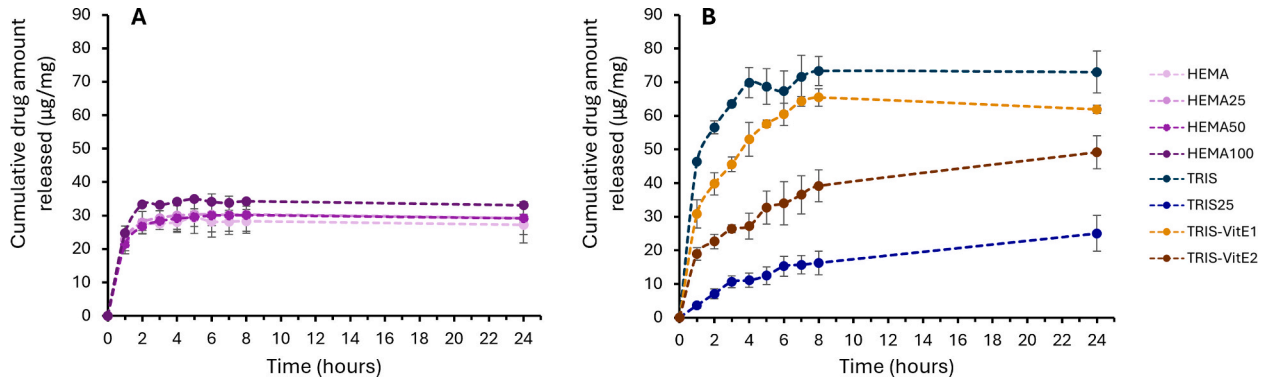

Fig. 1. Cumulative release of RA from (A) HEMA, HEMA25, HEMA50, HEMA100 and (B) TRIS, TRIS25, TRIS-VitE1 and TRIS-VitE2 in static conditions.

release kinetics without compromising the high RA-releasing capacity of TRIS hydrogels, these samples were subjected to a VitE pre-treatment. This resulted in an improvement in the release kinetics of the treated hydrogels, enabling a controlled drug release for 7 h and 24 h for TRIS-VitE1 and TRIS-VitE2 samples, respectively. All hydrogels released at least 70% of the drug amount loaded in the 24 h of the release experiment (Fig. S5Aii in Supplementary Information).

The described behaviour is in line with the work of other authors, who used VitE as a strategy to optimise the stability and control of the drug release from similar delivery systems. In fact, it has been reported that VitE accumulates at the interface between the hydrophilic phase of the hydrogel and its hydrophobic TRIS domains, (Quinn, 2007) acting as an inner barrier that increases the diffusional path of hydrophilic drugs across the material and, consequently, delays their release (Peng et al., 2010). For the same reason, if compared to the TRIS hydrogels, the incorporation of VitE decreased the cumulative drug amount released throughout the 24 h (≈15% and ≈ 30% lower for TRIS-VitE1 and TRIS-VitE2, respectively).

Based on these preliminary *in vitro* drug release results, TRIS-VitE1 hydrogels appeared as the most promising to be used as the material of RA-loaded daily CLs, as they enabled a 7 h controlled release whilst maintaining a high amount of eluted drug.

3.4. Drug amount loaded

Hydrogels loading was performed by soaking in RA solution in PBS. Although RA is hydrophilic, diffusion-based loading occurs because RA can form hydrogen bonds with the polymer chains and diffuses into the hydrated free volume of the hydrogel matrix. The amount of RA loaded onto each hydrogel is presented in Fig. 2. The TRIS-based hydrogels loaded the highest amount of RA, which is consistent with the results obtained from the molecular interaction analysis (section 3.2). However, the addition of APMA as a functional monomer to both HEMA and TRIS did not improve the drug loading.

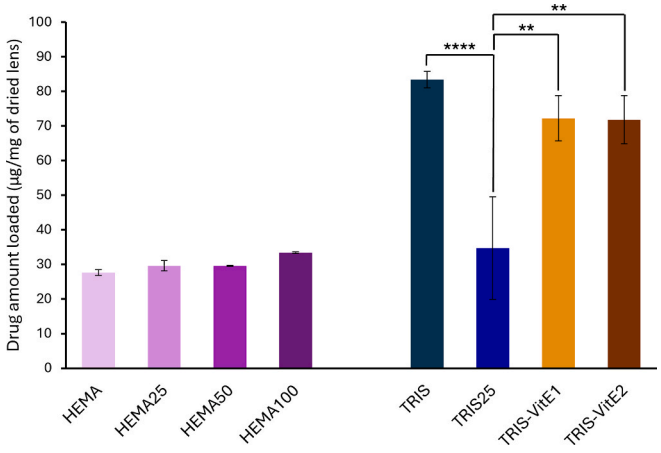

Fig. 2. Amount of RA loaded by each system, normalised by the weight of the dry hydrogel lens.

The obtained results for the acrylic hydrogels were consistent with the release profiles reported in Fig. 1A and demonstrated that, during the 24 h of release *in vitro*, the totality of the drug loaded was released from these hydrogels.

The VitE pre-treatment did not significantly alter RA loading onto the TRIS-based hydrogels. Based on the release profiles previously obtained from these hydrogels (Fig. 1B), it is possible to conclude that, with increasing doses of VitE, an increasing fraction of RA remains unreleased in the 24 h period of the test (≈15% for TRIS-VitE1 and ≈31% for TRIS-VitE2).

3.5. Characterisation of TRIS-VitE1 hydrogels

TRIS-VitE1 hydrogels, selected as the most promising system, were further characterised to ensure compliance with the required standards to be used as CLs. TRIS hydrogel was used as a control to investigate the effect of the VitE pre-treatment. The hydrogel's light transmittance, chemical composition, liquid uptake, wettability, surface morphology, and mechanical properties were assessed (Fig. 3).

All hydrogels' transmittance spectra were above 90% at wavelengths above 550 nm (Fig. 3A), which corresponds to the minimum requirement for CLs (Efron et al., 2011). The pre-treatment with VitE did not have any impact on the material's transmittance within the visible range.

The equilibrium swelling ratio (ESR) of the TRIS hydrogel in the RA loading solution assumed the value of 91 ± 7% (Fig. 3B), which can be attributed to the presence of the highly hydrophilic monomer NVP in the silicone hydrogels' structure (Maheswari et al., 2014). Such value is coherent with previously obtained data for the same hydrogel (Vivero-Lopez et al., 2021). VitE pre-treatment appears to have a tendency to lower the ESR of the hydrogel to 81 ± 7%, possibly due to the hydrophobic nature of VitE. Both values are higher than those found for commercial CLs (38–74%) (González-Méijome et al., 2006). However, hydrogels with ESR values in the 56–140% range have been previously reported as suitable CL materials (Vivero-Lopez et al., 2021).

The VitE-treated and non-treated hydrogels displayed a similar spectrum (Fig. 3C), with only minor alterations detected in the TRIS-VitE1 sample as small peaks around 1377 cm^{-1} and 2928 cm^{-1}, corresponding to C–H bending in the methyl group and the stretch of C–H in the methylene group, respectively (Coates, 2000; Pang et al., 2017). Since these bands were not observed in the non-treated samples and only in the pure VitE spectrum, it is reasonable to infer that the compound penetrated the polymer matrix and was the cause of these alterations in the chemical composition of the lens.

The SEM images of the TRIS hydrogel's surface revealed a smooth

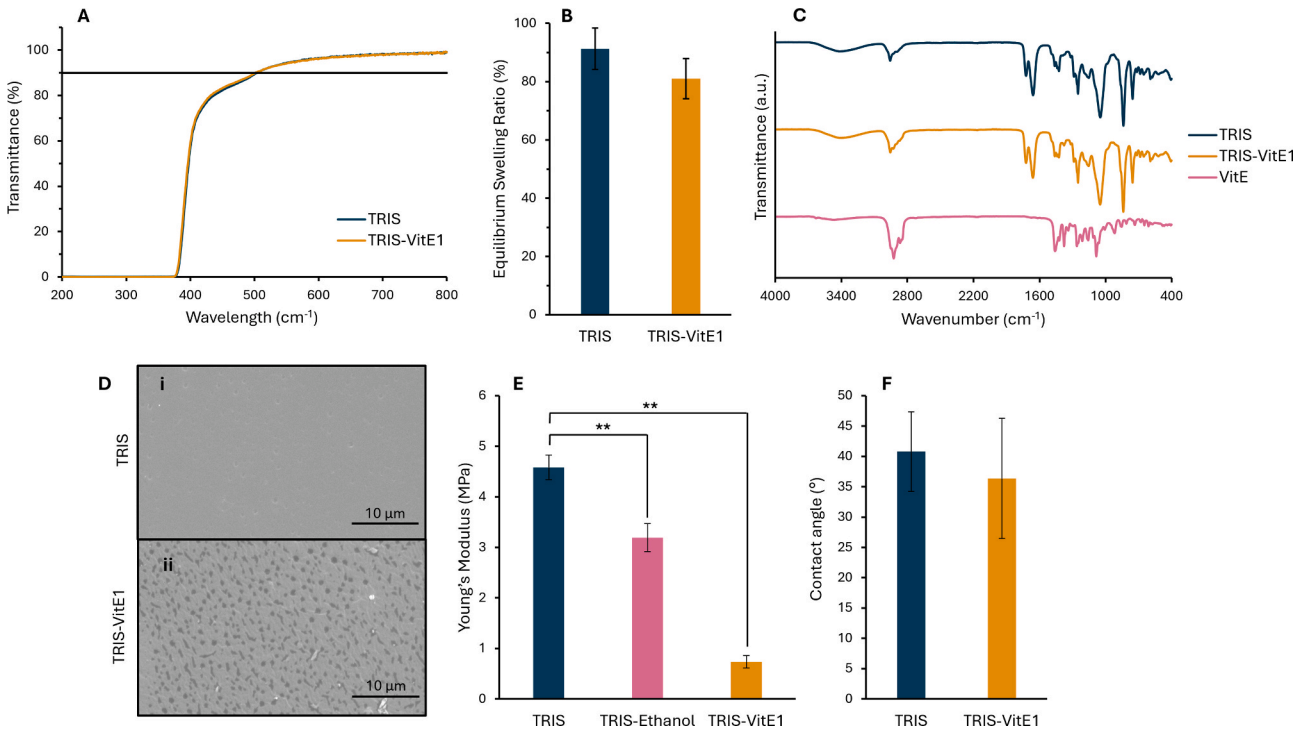

Fig. 3. Characterisation of TRIS and TRIS-VitE1 hydrogels. (A) Light transmittance after drug loading. The minimum light transmittance required for CLs (550 nm) is represented by the black line. (B) Equilibrium swelling ratio after drug loading. (C) FTIR-ATR spectra of the hydrogels and of pure VitE, in the region of 4000–400 cm^{-1}. (D) SEM images of the surface of the TRIS and TRIS-VitE1 hydrogels at amplification 3500x. (E) Young's modulus of PBS-hydrated TRIS, TRIS-Ethanol and TRIS-VitE1 hydrogels. (F) Water contact angle of hydrated TRIS and TRIS-VitE1 hydrogels.

homogeneous surface (Fig. 3Di). After pre-treatment in VitE, distinct spots appeared on the hydrogels' surface (Fig. 3Dii), which were identified as VitE aggregates (Dixon et al., 2018).

The hydrogels' Young's moduli (Fig. 3E) were obtained in tensile tests to infer whether the VitE treatment impacted the material's stiffness. TRIS hydrogels exhibited an elastic modulus of 4.6 ± 0.2 MPa, which is significantly above the values reported for commercial silicone CLs (0.3–1.9 MPa) and could cause eye irritation (Efron et al., 2011). The addition of VitE significantly decreased the Young's modulus to a value of 0.7 ± 0.1 MPa, which is comparable with commercial CLs. As the VitE pre-treatment is performed in ethanol, the effect of the solvent *per si* was also hypothesised, and TRIS-samples pre-soaked in ethanol were also tested. The results indicate that although ethanol contributed to the reduction, VitE further reduced the Young's modulus. In fact, the presence of VitE could hinder the chain-chain interactions of the polymer, therefore increasing its elasticity.

The static contact angle of hydrated TRIS and TRIS-VitE1 samples resulted equal to 41 ± 7° and 36 ± 10°, respectively, with no statistical difference between the two (Fig. 3F). Such values indicate the hydrophilic nature of the surfaces (Law, 2014), regardless of the presence of VitE. These results are consistent with previous data reported in the literature for these hydrogels (Paradiso et al., 2016).

3.6. Biocompatibility study

The effect of sterilisation on the TRIS hydrogels, prior to the VitE pre-treatment, is reported in Supplementary Fig. S6. Briefly, autoclaving did not alter the chemical structure and mechanical properties of the material. The hydrogels were then loaded with VitE in sterile conditions. The drug release profile was not affected by the previous sterilisation of the hydrogel (data not shown). Thus, autoclaving was adopted as sterilisation method of the hydrogels to ensure the biological safety of the system.

In vitro viability of human corneal cells in the presence of TRIS-VitE1 hydrogels either loaded or unloaded with RA, was 86.6 ± 22.5% and 95.7 ± 8.9%, respectively (Fig. 4Ai), which means that both systems can be considered non-cytotoxic according to the ISO 10993–5: 2009 standard (ISO 10993–5, 2009) Additional testing with dilutions of a fresh RA solution (Fig. 4Aii) allowed us to identify a RA concentration of 625 µg/mL as the cytotoxicity threshold, which is comparable to literature values (Vieira et al., 2020).

The HET-CAM assay has been performed to determine the ocular irritability of the designed systems, as the CAM blood vessels have similarities to the vasculature of the ocular conjunctiva (Budai et al., 2021). Images of the CAM exposed to the samples (Fig. 4B) suggest that both RA-loaded and unloaded hydrogels shall not be irritant for the ocular surface, as no signs of haemorrhage, lysis or coagulation were observed within the duration of the test.

3.7. Prediction of ocular drug distribution based on in vitro and ex vivo data

To provide an estimation of ocular drug distribution *in vivo* after CL wearing, *in vitro* release data and *ex vivo* permeability results were integrated into a previously developed mathematical model. This approach provides a theoretical prediction that supports the optimization and selection of the most promising hydrogels prior to *in vivo* studies; it does not constitute a direct *in vivo* measurement nor aims to replace *in vivo* experiments.

3.7.1. Hydrodynamic drug release

Drug release experiments were performed in a release medium volume lower than that used in static conditions (section 3.3) and with continuous renovation of the medium at a constant rate, allowing for an approximation to the hydrodynamic functioning of the eye. Compared to the drug release profile obtained in static conditions, a more gradual and sustained release of RA was observed during the 24 h assay (Fig. 5A). While in static conditions ≈ 90% of the loaded drug was

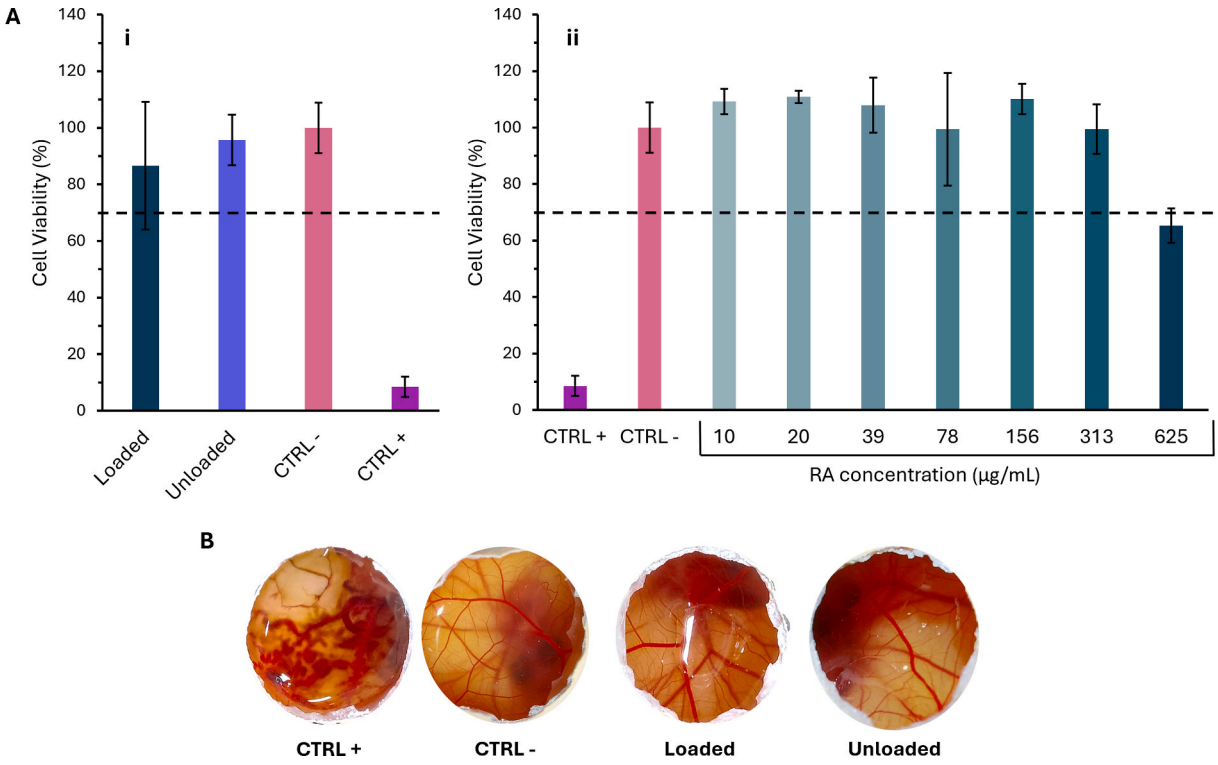

Fig. 4. (A) Human primary corneal epithelial cells viability tested through: (i) indirect contact with RA-loaded and unloaded TRIS-VitE1 hydrogels (ii) incubation with different concentrations of a fresh RA solution (from 10 to 625 µg/mL) (n = 3). The minimum cell viability required to be non-cytotoxic (70%) is represented by the black dotted line. (Positive control: cells + culture medium with 10% DMSO; negative control: cells + culture medium). (B) Representative images of HET-CAM after a 5-minute exposure to the positive control, negative control, RA-loaded and non-loaded TRIS-VitE1 hydrogels. (Positive control: 1 M NaOH; negative control: 0.9% NaCl).

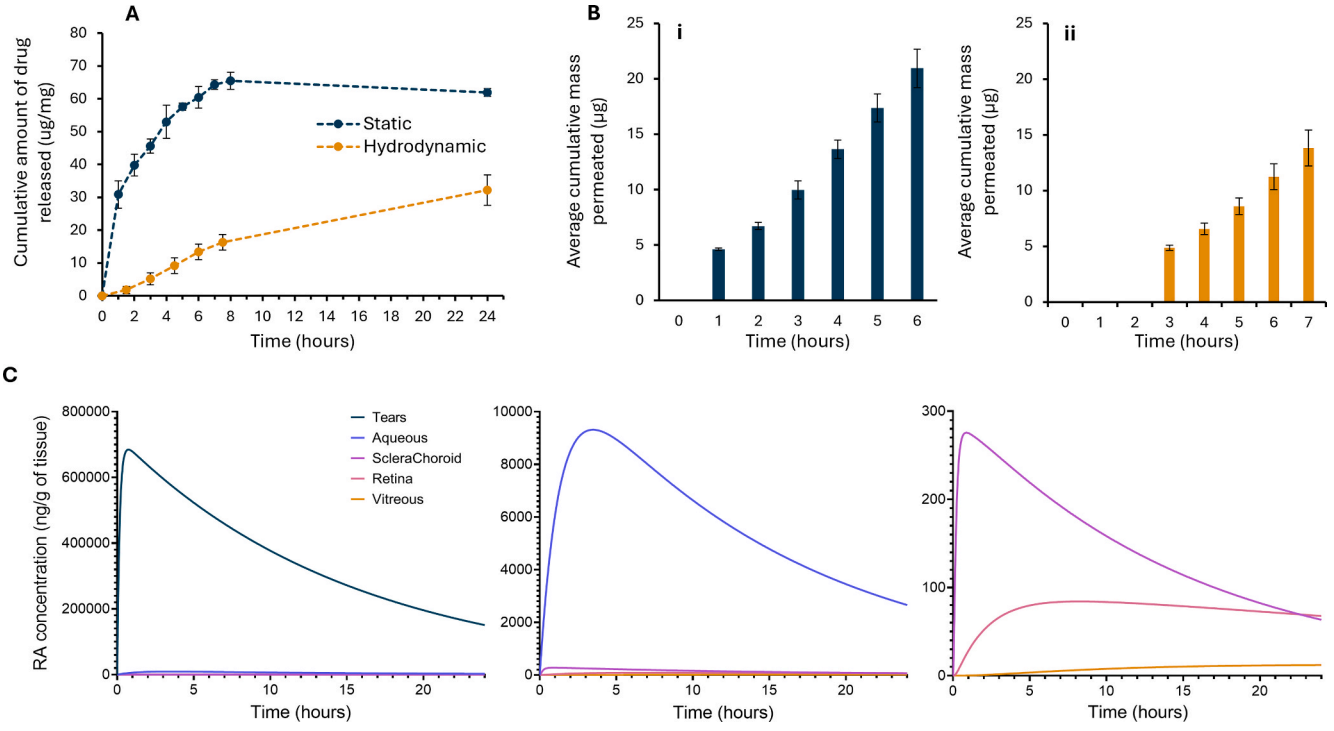

Fig. 5. Estimation of *in vivo* behaviour. (A) Comparison between the release profile of RA from TRIS-VitE1 hydrogels in static and hydrodynamic conditions, indicated as µg released per mg of dry hydrogel. (B) Drug amount permeated across the (i) cornea and (ii) sclera over time. (C) Predicted drug concentration in the eye after wearing of a loaded TRIS-VitE1 CL, zoomed representations are shown on the right.

released by the end of the experiment (24 h), in hydrodynamic conditions this percentage was lowered to ≈ 40% (Fig. S5B in

Supplementary information). The use of a smaller release volume (45 μL instead of 3 mL) decreased the concentration gradient between the release medium and the hydrogel, resulting in a lower diffusion rate. This is also the reason why the amount of RA released during 24 h was much lower (≈ 32 μg/mg of dried lens, compared to the ≈ 62 μg/mg released under static settings). Looking at the slope of the release curve obtained in hydrodynamic conditions, a plateau was not achieved within the 24 h of the test, which suggests longer release times may be achieved *in vivo*.

3.7.2. Ex vivo permeability evaluation

The cumulative amount of RA that permeates across the cornea and the sclera along the first 6–7 h of contact with drug solutions is presented in Fig. 5B. The scleral permeability of RA was found to be 3.4 ± 0.5 × 10^{-6} cm/s, which falls within the range of permeability values reported in the literature (0.5–7 × 10^{-6} cm/s) for drugs of similar molecular weight and lipophilicity (log$D_{7.4}$ values) (Pereira-da-Mota et al., 2022; Prausnitz et al., 1998).

Conversely, the corneal permeability (5.0 ± 0.5 x 10^{-6} cm/s) was above the reported values for similar drugs (0.1–2 × 10^{-6} cm/s) (Ramsay et al., 2018). The permeability coefficients for ocular tissues vary greatly in the literature due to differing setups, test conditions and quantification techniques. However, a higher permeability across the cornea, when compared to the sclera, is unusual as the cornea's epithelial tight junctions generally hinder drug diffusion. Although RA is considered a hydrophilic molecule (multiple hydroxyl groups), its aromantic rings suggest some lipophilic potential. The drug's nature could therefore aid its crossing through both lipophilic (epithelium and endothelium) and hydrophilic (stroma) corneal layers. Moreover, RA exhibited a higher affinity for the sclera than the cornea, as shown by their partition coefficient values (K = 3.9 ± 0.1 and K = 8.1 ± 0.6 for the cornea and sclera, respectively), which may lead to the accumulation of RA in the sclera and a potential delay in its permeation through this tissue.

3.7.3. Modelling ocular drug distribution

The drug concentration in the different segments of the eye after applying the RA-loaded SCLs was estimated using a previously developed mathematical model (Toffoletto et al., 2023). The simulation was done by using as an input the exponential fitting of the *in vitro* hydrodynamic release profile (Supplementary Fig. S7), as this is expected to better mimic the release conditions in the eye. Other drug-specific input values for the model are reported in Table S1.

Regarding the posterior segment of the eye, RA retinal concentration is expected to reach a peak of 86 ng/g of tissue, 6 h after application of the therapeutic CL, followed by a slow decline (Fig. 5C). Although no minimal therapeutic concentrations have been reported in the literature for retinal pathologies, RA has been documented to have neuroprotective effects, which are desirable for the management of several retinal pathologies, at a concentration as low as 1 nM (0.36 ng/mL) (Du et al., 2010), which suggests a potential protective effect of the designed RA-eluting CLs. Regarding antioxidant and anti-inflammatory activity, a concentration of 1 μM (360 ng/mL) was found to be effective (Ku et al., 2013; Lu et al., 2017). To determine the minimum antioxidant concentration of RA, an *in vitro* test was performed in the present work (Section 3.8.1), while the minimum neuroprotective concentration of RA was assessed by an *ex vivo* assay on porcine retina (Section 3.8.2).

In the anterior segment of the eye, RA concentration in the aqueous humour is expected to reach a peak of 9 μg/mL, indicating that RA would be able to counter oxidative stress and inflammation, thus protecting the crystallin of diabetic patients from complications such as cataracts (Bron et al., 1993). Furthermore, it has been reported that exposure to 12.5 μM (4.5 μg/mL) of RA effectively inhibits crucial stages of angiogenesis (Huang et al., 2006). Although neovascularisation issues are more frequently associated with the posterior segment of the eye, an anti-angiogenic effect is desired to counteract pathologies such as neovascular glaucoma, which affects the iris (Tang et al., 2023).

RA concentration in all ocular tissues is estimated to remain below the cytotoxicity limit (625 μg/mL on human corneal epithelial cells, Section 3.6), with only a slightly higher value predicted in tears at peak concentration (658 μg/mL). Notably, the drug concentration in tears is expected to decrease below the cytotoxicity limit after the first 3 h of CL wear (Fig. 5C), whereas *in vitro* cytotoxicity tests were performed over 24 h. Therefore, it is plausible that corneal cells could tolerate the transiently elevated RA levels in tears during the initial hours of CL wear. *In vivo* studies would be valuable to ascertain if corneal cells can tolerate prolonged exposure to RA at such doses.

3.8. RA's therapeutic activity

3.8.1. Antioxidant effect

A DPPH assay was performed to assess the antioxidant capacity of the drug released from the TRIS-VitE1 hydrogels and examine if RA's therapeutic activity was impacted by the loading and release process.

A scavenging effect of 75 ± 2% was observed at a concentration of 50 μg/mL (Fig. 6), demonstrating the antioxidant potential of the system. As a comparison, a study on resveratrol-releasing hydrogels considered the system to have an antioxidant effect when the scavenging effect was between 26 ± 5% and 59 ± 2% (Vivero-Lopez et al., 2021). Dilutions of released RA were tested down to a minimum of 3 μg/mL, which presented 28 ± 6% scavenging effect. This confirmed the antioxidant potential of the designed system in the tears and aqueous humour, where the estimated drug concentration shall reach peaks of 685 μg/mL and 9 μg/mL, respectively (section 3.7.3). Additionally, a comparison between the scavenging effect of fresh RA solutions and RA released from the hydrogels revealed that the antioxidant potential was not significantly affected by the loading and release processes.

To predict if any additional antioxidant effect may take place *in vivo* due to the presence of VitE (a known antioxidant) (Li et al., 2024) domains in the hydrogel, the supernatants of TRIS and TRIS-VitE1 hydrogels were also submitted to the DPPH test. However, no significant effect was found after the hydrogel's pre-treatment in VitE (Fig. 6). Nevertheless, in the ocular environment, this molecule could still potentially contribute to the contact lenses' antioxidant activity. Although it does not diffuse from the hydrogel, it may aid in scavenging radical species that diffuse into the CL matrix.

3.8.2. Neuroprotective effect

In a diabetic context, there will be a progressive loss of the retinal ganglion cells (RGCs) (Potilinski et al., 2020). To confirm the neuroprotective effect of RA, an *ex vivo* assay was conducted to evaluate the preservation of RGCs ($Brn3a^+$ cells) in porcine retinal explants after 2 days of RA treatment (Fig. 7).

The 2-day incubation of the explants (D2) resulted in a significant decrease in the number of $Brn3a^+$ cells compared to D0, indicating the occurrence of neurodegeneration (Meng et al., 2024). However, the retinal explants treated with RA showcased an improvement in RGC survival compared to D2, with $Brn3a^+$ cells tending to approach those observed at D0. This suggests a preservation or recovery of functional RGCs and reinforces the neuroprotective potential of RA, as previously documented (Du et al., 2010; Fallarini et al., 2009; Le et al., 2021). RA's neuroprotective effect appears to be concentration-dependent, with a tendency for increased efficacy at higher concentrations. At a concentration of 86 ng/mL, the drug already tended to have a protective effect compared to D2, but at 400 ng/mL, RA demonstrated a pronounced neuroprotective outcome. Although the estimated peak concentration of RA in the retina is 86 ng/mL (section 3.7.3), it was noted that in this tissue the drug turnover is slow. This implies that, as the RA-eluting SCLs are to be replaced daily, the drug could gradually accumulate in the retina and, after approximately 4 to 5 days, reach concentrations able to exert a substantial neuroprotective effect.

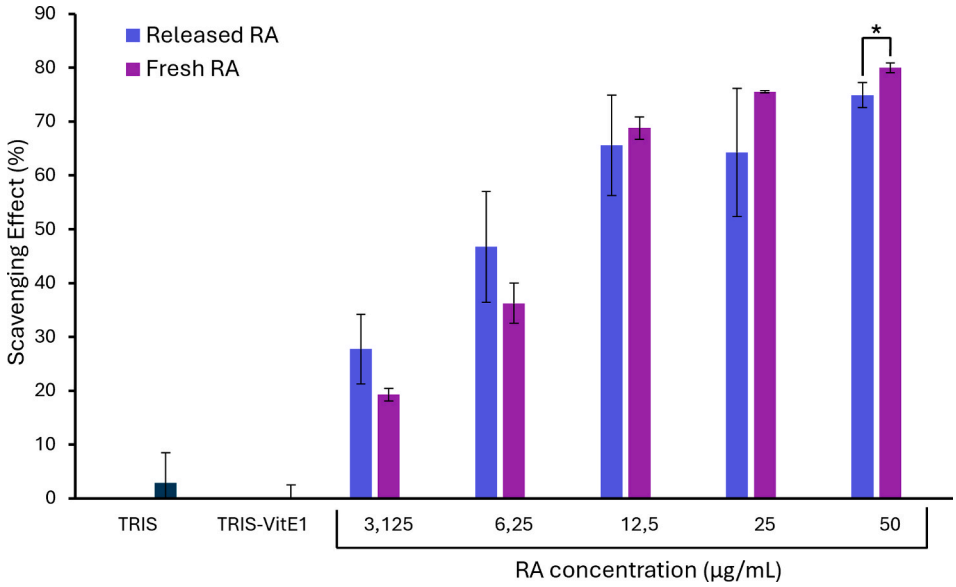

Fig. 6. Scavenging effect of RA solutions, either released from the hydrogel or freshly prepared. Dilutions from 50 to 3.13 µg/mL of RA were tested. The supernatants of non-loaded samples (TRIS and TRIS-VitE1) were also analysed as control.

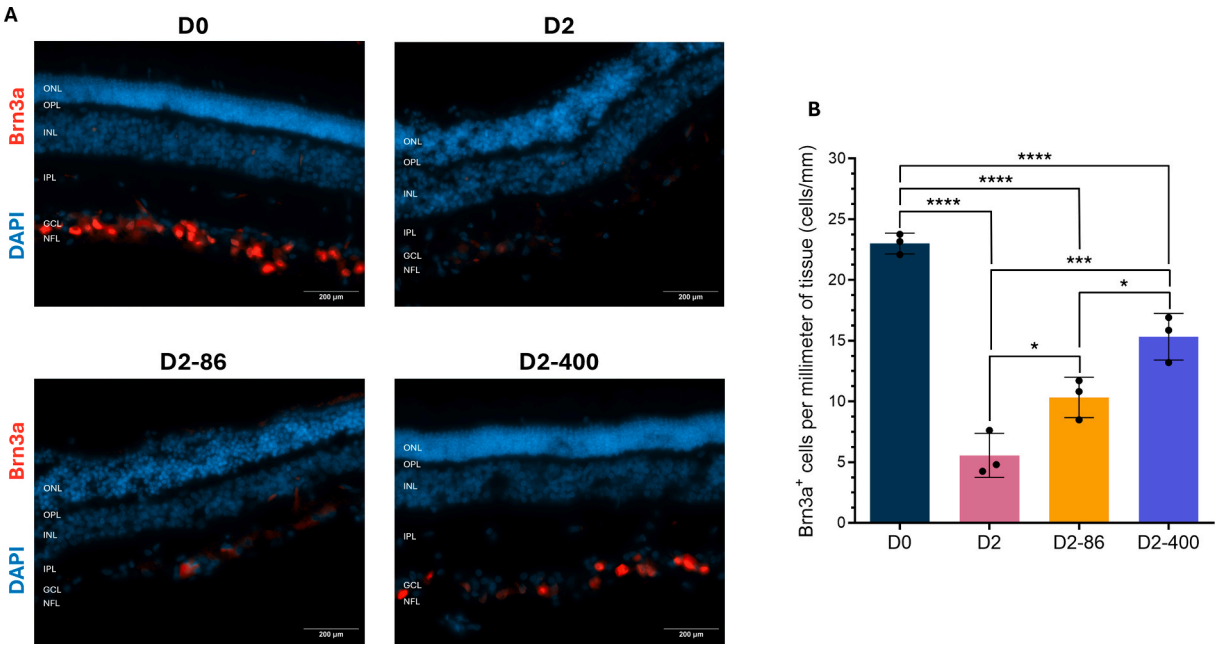

Fig. 7. Assessment of RA neuroprotective activity in *ex vivo* porcine retina cultures. (A) Representative immunofluorescence staining for RGC ($Brn3a^+$ cells, in red) and nuclei (DAPI, in blue) on retinal sections of porcine explants at day 0 (D0) or after 2 days in culture, without (D2) or with treatment of RA at 86 ng/mL (D2-86) or 400 ng/mL (D2-400) (Scale bar = 200 µm); ONL (outer nuclear layer), OPL (outer plexiform layer), INL (inner nuclear layer), IPL (inner plexiform layer), GCL (ganglion cell layer) and NFL (nerve fibre layer). (B) Quantification of $Brn3a^+$ cells across the GCL. Data represent mean ± SD of 3 independent experiments, with at least 10 images per condition.

4. Conclusions

This work aimed to develop a simple-to-manufacture hydrogel able to release RA, a natural polyphenol, to be used in therapeutic CLs for the treatment of diabetic ocular complications.

Both acrylic and silicone-based hydrogels were produced, with the optimal release kinetics being obtained with the silicone-based hydrogels pre-treated with VitE. This specific system demonstrated a controlled release profile for up to 7 h in sink conditions and 24 h under hydrodynamic conditions, which more closely resembled the ocular environment. The hydrogel's physical, chemical and biological properties were assessed to ensure their suitability as commercial CLs. Importantly, the material maintained high transparency above 550 nm, while filtering UV radiation and blue light, which can potentially exert harmful effects on the eye. The system also presented a hydrophilic surface and an equilibrium water content that ensures the required comfort for the user. Moreover, the TRIS-VitE1 hydrogels showed a suitable stiffness. Regarding biocompatibility, the system revealed no signs of cytotoxicity or irritation. By performing an *ex vivo* permeability study, RA's ability to diffuse across the cornea and sclera was confirmed. With the obtained permeability parameters, a drug distribution simulation was conducted, which predicted therapeutically relevant

concentrations in the target ocular tissues. The drug's bioactivity appears to be unaffected by the loading and release processes, as the released RA still demonstrated a strong antioxidant activity. Tests on the neuroprotective also revealed that, with the accumulation of RA in the retina, the system has the potential to reach relevant concentrations for the preservation of the RGC layer.

Altogether, the TRIS-VitE1 hydrogels developed in this study offer a promising platform for the sustained delivery of RA in the treatment of diabetic-related ocular pathologies. This therapeutic device not only holds significant potential for improving ocular clinical outcomes but also for enhancing the quality of life for patients struggling with the chronic challenges of diabetes.

Future work will involve the production of the hydrogels in curved contact lens moulds, allowing the assessment of contact-lens–specific parameters such as curvature stability, refractive power, and corneal fitting, particularly after drug loading and release. Anti-inflammatory activity evaluation tests on appropriate retinal cell lines should also be performed to further characterize the therapeutic effect of the device.

CRediT authorship contribution statement

Ana Centeno Duarte: Writing – original draft, Methodology, Investigation, Formal analysis. **Nadia Toffoletto:** Writing – review & editing, Writing – original draft, Validation, Supervision, Methodology, Investigation, Formal analysis, Conceptualization. **Rita Martins Pais:** Writing – original draft, Methodology, Investigation, Formal analysis, Data curation. **Zélia Lumack do Monte:** Methodology, Investigation, Formal analysis. **Madalena Salema-Oom:** Writing – review & editing, Validation, Methodology, Investigation, Data curation. **Sandra Tenreiro:** Writing – review & editing, Validation, Supervision, Formal analysis. **Ana Paula Serro:** Writing – review & editing, Supervision, Resources, Project administration, Methodology, Investigation, Funding acquisition, Formal analysis, Conceptualization.

Declaration of competing interest

The authors declare that they have no known competing financial interests or personal relationships that could have appeared to influence the work reported in this paper.

Acknowledgments

The authors acknowledge Fundação para a Ciência e a Tecnologia (FCT) for funding through the project SOL - Smart ocular lenses for the treatment of diabetic eye diseases (https://doi.org/10.54499/PTDC/CTM-CTM/2353/2021), and through projects of CQE - Centro de Química Estrutural (UID/00100/2025 and UID/PRR/100/2025), of the Associate Laboratory IMS - Institute of Molecular Sciences (https://doi.org/10.54499/LA/P/0056/2020), of iNOVA4Health (https://doi.org/10.54499/UIDB/04462/2020 and https://doi.org/10.54499/UIDP/04462/2020), of the Associated Laboratory LS4FUTURE (https://doi.org/10.54499/LA/P/0087/2020), and the PhD grant 2024.02715.BD (RMP). Acknowledgements are also due to Dr. Diana Silva and Eng. João Teixeira for helping with FTIR analysis and antioxidant activity tests, respectively. We also acknowledge Paulo Pinheiro from CASO (Centro de Abate de Suínos do Oeste) and Eng. Humberto Marques and Dr. Maria do Carmo Silva from SICASAL - Indústria e Comércio de Carnes for generously providing the excised porcine eyes. Furthermore, the authors thank UTR-C2TN (Eng. Paula Matos) for performing the gamma irradiation of the material used in the cytotoxicity tests.

Appendix A. Supplementary data

Supplementary data to this article can be found online at https://doi.org/10.1016/j.ijpharm.2026.126591.

Data availability

Data will be made available on request.

References

Agrahari, V., Mandal, A., Agrahari, V., Trinh, H.M., Joseph, M., Ray, A., Hadji, H., Mitra, R., Pal, D., Mitra, A.K., 2016. A comprehensive insight on ocular pharmacokinetics. Drug Deliv. Transl. Res. 6 (6), 735–754. https://doi.org/10.1007/s13346-016-0339-2.

Bachu, R., Chowdhury, P., Al-Saedi, Z., Karla, P., Boddu, S., 2018. Ocular drug delivery barriers—role of nanocarriers in the treatment of anterior segment ocular diseases. Pharmaceutics 10 (1), 28. https://doi.org/10.3390/pharmaceutics10010028.

Banday, M.Z., Sameer, A.S., Nissar, S., 2020. Pathophysiology of diabetes: an overview. Avicenna Journal of Medicine 10 (4), 174–188. https://doi.org/10.4103/ajm.ajm_53_20.

Biswas, M., Haldar, P.K., Ghosh, A.K., 2010. Antioxidant and free-radical-scavenging effects of fruits of Dregea volubilis. Journal of Natural Science, Biology, and Medicine 1 (1), 29–34. https://doi.org/10.4103/0976-9668.71670.

Bron, A.J., Sparrow, J., Brown, N.A.P., Harding, J.J., Blakytny, R., 1993. The lens in diabetes. Eye 7 (2), 260–275. https://doi.org/10.1038/eye.1993.60.

Budai, P., Kormos, É., Buda, I., Somody, G., Lehel, J., 2021. Comparative evaluation of HET-CAM and ICE methods for objective assessment of ocular irritation caused by selected pesticide products. Toxicol. In Vitro 74, 105150. https://doi.org/10.1016/j.tiv.2021.105150.

Carnahan, M.C., Goldstein, D.A., 2000. Ocular complications of topical, peri-ocular, and systemic corticosteroids. Curr. Opin. Ophthalmol. 11 (6), 478–483. https://doi.org/10.1097/00055735-200012000-00016.

Chawan-Saad, J., Wu, M., Wu, A., Wu, L., 2019. Corticosteroids for diabetic macular edema. Taiwan Journal of Ophthalmology 9 (4), 233. https://doi.org/10.4103/tjo.tjo_68_19.

Chemerovski-Glikman, M., Mimouni, M., Dagan, Y., Haj, E., Vainer, I., Allon, R., Blumenthal, E.Z., Adler-Abramovich, L., Segal, D., Gazit, E., Zayit-Soudry, S., 2018. Rosmarinic acid restores complete transparency of sonicated human cataract Ex vivo and delays cataract formation in vivo. Sci. Rep. 8 (1), 9341. https://doi.org/10.1038/s41598-018-27516-9.

ChemSpider. (n.d.). *(R)-(+)-rosmarinic acid (CSID:4445104)*. https://Www.Chemspider.Com/Chemical-Structure.4445104.Html.

Chen, Y.-Y., Tsai, C.-F., Tsai, M.-C., Hsu, Y.-W., Lu, F.-J., 2017. Inhibitory effects of rosmarinic acid on pterygium epithelial cells through redox imbalance and induction of extrinsic and intrinsic apoptosis. Exp. Eye Res. 160, 96–105. https://doi.org/10.1016/j.exer.2017.05.008.

Coates, J. (2000). Interpretation of infrared spectra, a practical approach. In Encyclopedia of analytical chemistry (Vol. 12, pp. 10815–10837).

da Silva, S.B., Ferreira, D., Pintado, M., Sarmento, B., 2016. Chitosan-based nanoparticles for rosmarinic acid ocular delivery—In vitro tests. Int. J. Biol. Macromol. 84, 112–120. https://doi.org/10.1016/j.ijbiomac.2015.11.070.

Dewan, L., Loomis, C.A., 2016. Tissue preparation and cryopreservation with sucrose: for frozen tissue sections. Exp Pathol Res Lab 1–2.

Dixon, P., Ghosh, T., Mondal, K., Konar, A., Chauhan, A., Hazra, S., 2018. Controlled delivery of pirfenidone through vitamin E-loaded contact lens ameliorates corneal inflammation. Drug Deliv. Transl. Res. 8 (5), 1114–1126. https://doi.org/10.1007/s13346-018-0541-5.

Du, T., Li, L., Song, N., Xie, J., Jiang, H., 2010. Rosmarinic acid antagonized 1-Methyl-4-Phenylpyridinium (MPP +)-induced neurotoxicity in MES23.5 dopaminergic cells. Int. J. Toxicol. 29 (6), 625–633. https://doi.org/10.1177/1091581810383705.

Du, X., Li, Y., Xia, Y.-L., Ai, S.-M., Liang, J., Sang, P., Ji, X.-L., Liu, S.-Q., 2016. Insights into protein–ligand interactions: mechanisms, models, and methods. Int. J. Mol. Sci. 17 (2), 144. https://doi.org/10.3390/ijms17020144.

Efron, N., & Maldonado-Codina, C. (2011). Development of Contact Lenses from a Biomaterial Point of View – Materials, Manufacture, and Clinical Application. In Comprehensive Biomaterials (pp. 517–541). Elsevier. doi: 10.1016/B978-0-08-055294-1.00270-1.

El-Huneidi, W., Anjum, S., Mohammed, A.K., Bin Eshaq, S., Abdrabh, S., Bustanji, Y., Soares, N.C., Semreen, M.H., Alzoubi, K.H., Abu-Gharbieh, E., Taneera, J., 2023. Rosemarinic acid protects β-cell from STZ-induced cell damage via modulating NF-κβ pathway. Heliyon 9 (9), e19234. https://doi.org/10.1016/j.heliyon.2023.e19234.

Fachel, F.N.S., Schuh, R.S., Veras, K.S., Bassani, V.L., Koester, L.S., Henriques, A.T., Braganhol, E., Teixeira, H.F., 2019. An overview of the neuroprotective potential of rosmarinic acid and its association with nanotechnology-based delivery systems: a novel approach to treating neurodegenerative disorders. Neurochem. Int. 122, 47–58. https://doi.org/10.1016/j.neuint.2018.11.003.

Fallarini, S., Miglio, G., Paoletti, T., Minassi, A., Amoruso, A., Bardelli, C., Brunelleschi, S., Lombardi, G., 2009. Clovamide and rosmarinic acid induce neuroprotective effects in *in vitro* models of neuronal death. Br. J. Pharmacol. 157 (6), 1072–1084. https://doi.org/10.1111/j.1476-5381.2009.00213.x.

Galante, R., Oliveira, A.S., Topete, A., Ghisleni, D., Braga, M., Pinto, T.J.A., Colaço, R., Serro, A.P., 2018. Drug-eluting silicone hydrogel for therapeutic contact lenses: Impact of sterilization methods on the system performance. Colloids Surf. B Biointerfaces 161, 537–546. https://doi.org/10.1016/j.colsurfb.2017.11.021.

Gause, S., Hsu, K.-H., Shafor, C., Dixon, P., Powell, K.C., Chauhan, A., 2016. Mechanistic modeling of ophthalmic drug delivery to the anterior chamber by eye drops and contact lenses. Adv. Colloid Interface Sci. 233, 139–154. https://doi.org/10.1016/j.cis.2015.08.002.

Glasson, M.J., Stapleton, F., Keay, L., Willcox, M.D.P., 2006. The effect of short term contact lens wear on the tear film and ocular surface characteristics of tolerant and intolerant wearers. Contact Lens and Anterior Eye 29 (1), 41–47. https://doi.org/10.1016/j.clae.2005.12.006.

González-Méijome, J.M., Lira, M., López-Alemany, A., Almeida, J.B., Parafita, M.A., Refojo, M.F., 2006. Refractive index and equilibrium water content of conventional and silicone hydrogel contact lenses. Ophthalmic Physiol. Opt. 26 (1), 57–64. https://doi.org/10.1111/j.1475-1313.2005.00342.x.

Govindaraj, J., Sorimuthu Pillai, S., 2015. Rosmarinic acid modulates the antioxidant status and protects pancreatic tissues from glucolipotoxicity mediated oxidative stress in high-fat diet: streptozotocin-induced diabetic rats. Mol. Cell. Biochem. 404 (1–2), 143–159. https://doi.org/10.1007/s11010-015-2374-6.

Han, S.B., Yang, H.K., Hyon, J.Y., 2018. Influence of diabetes mellitus on anterior segment of the eye. Clin. Interv. Aging 14, 53–63. https://doi.org/10.2147/CIA.S190713.

Hsu, K.-H., Carbia, B.E., Plummer, C., Chauhan, A., 2015. Dual drug delivery from vitamin E loaded contact lenses for glaucoma therapy. Eur. J. Pharm. Biopharm. 94, 312–321. https://doi.org/10.1016/j.ejpb.2015.06.001.

Huang, S., Zheng, R., 2006. Rosmarinic acid inhibits angiogenesis and its mechanism of action in vitro. Cancer Lett. 239 (2), 271–280. https://doi.org/10.1016/j.canlet.2005.08.025.

ICCVAM. (2010). ICCVAM-Recommended test method protocol: Hen's Egg Test—Chorioallantoic Membrane (HET-CAM) test method. *NIH Publication 13 , B30-8*.

Inui, A., Cheng, K.-C., Asakawa, A., Amitani, H., Amitani, M., Morinaga, A., Takimoto, Y., Kairupan, B.H.R., Runtuwene, J., 2016. Rosmarinic acid ameliorates hyperglycemia and insulin sensitivity in diabetic rats, potentially by modulating the expression of PEPCK and GLUT4. Drug Des. Devel. Ther. 10, 2193–2202. https://doi.org/10.2147/DDDT.S108539.

ISO. (2009). *10993–5: 2009 Biological evaluation of medical devices—part 5: tests for in vitro cytotoxicity*. Geneva: International Organization for Standardization.

Kattar, A., Concheiro, A., Alvarez-Lorenzo, C., 2021. Diabetic eye: associated diseases, drugs in clinic, and role of self-assembled carriers in topical treatment. Expert Opin. Drug Deliv. 18 (11), 1589–1607. https://doi.org/10.1080/17425247.2021.1953466.

Khojasteh, A., Mirjalili, M.H., Alcalde, M.A., Cusido, R.M., Eibl, R., Palazon, J., 2020. Powerful plant antioxidants: a new biosustainable approach to the production of rosmarinic acid. Antioxidants 9 (12), 1273. https://doi.org/10.3390/antiox9121273.

Kim, H.M., Han, H., Hong, H.K., Park, J.H., Park, K.H., Kim, H., Woo, S.J., 2021. Permeability of the retina and RPE-choroid-sclera to three ophthalmic drugs and the associated factors. Pharmaceutics 13 (5), 655. https://doi.org/10.3390/pharmaceutics13050655.

Kim, J.H., Lee, B.J., Kim, J.H., Yu, Y.S., Kim, M.Y., Kim, K.-W., 2009. Rosmarinic acid suppresses retinal neovascularization via cell cycle arrest with increase of p21WAF1 expression. Eur. J. Pharmacol. 615 (1–3), 150–154. https://doi.org/10.1016/j.ejphar.2009.05.015.

Kim, S.J., Flach, A.J., Jampol, L.M., 2010. Nonsteroidal anti-inflammatory drugs in ophthalmology. Surv. Ophthalmol. 55 (2), 108–133. https://doi.org/10.1016/j.survophthal.2009.07.005.

Kim, S., Thiessen, P.A., Bolton, E.E., Chen, J., Fu, G., Gindulyte, A., Han, L., He, J., He, S., Shoemaker, B.A., Wang, J., Yu, B., Zhang, J., Bryant, S.H., 2016. PubChem substance and compound databases. Nucleic Acids Res. 44 (D1), D1202–D1213. https://doi.org/10.1093/nar/gkv951.

Kropp, M., Golubnitschaja, O., Mazurakova, A., Koklesova, L., Sargheini, N., Vo, T.-T.-K.-S., de Clerck, E., Polivka, J., Potuznik, P., Polivka, J., Stetkarova, I., Kubatka, P., Thumann, G., 2023. Diabetic retinopathy as the leading cause of blindness and early predictor of cascading complications—risks and mitigation. EPMA Journal 14 (1), 21–42. https://doi.org/10.1007/s13167-023-00314-8.

Ku, S.-K., Yang, E.-J., Song, K.-S., Bae, J.-S., 2013. Rosmarinic acid down-regulates endothelial protein C receptor shedding in vitro and in vivo. Food Chem. Toxicol. 59, 311–315. https://doi.org/10.1016/j.fct.2013.06.003.

Law, K.-Y., 2014. Definitions for hydrophilicity, hydrophobicity, and superhydrophobicity: getting the basics right. The Journal of Physical Chemistry Letters 5 (4), 686–688. https://doi.org/10.1021/jz402762h.

Le, T.T., Kang, T.K., Do, H.T., Nghiem, T.D., Lee, W.-B., Jung, S.H., 2021. Protection against oxidative stress-induced retinal cell death by compounds isolated from *Ehretia asperula*. Nat. Prod. Commun. 16 (12). https://doi.org/10.1177/1934578X211067986.

Li, C.-Y., Lin, W.-C., Moonmanee, T., Chan, J.-P.-W., Wang, C.-K., 2024. The protective role of Vitamin E against oxidative stress and immunosuppression induced by non-esterified fatty acids in bovine peripheral blood leukocytes. Animals 14 (7), 1079. https://doi.org/10.3390/ani14071079.

Lu, C., Zou, Y., Liu, Y., Niu, Y., 2017. Rosmarinic acid counteracts activation of hepatic stellate cells via inhibiting the ROS-dependent MMP-2 activity: Involvement of Nrf2 antioxidant system. Toxicol. Appl. Pharmacol. 318, 69–78. https://doi.org/10.1016/j.taap.2017.01.008.

Luo, C., Zou, L., Sun, H., Peng, J., Gao, C., Bao, L., Ji, R., Jin, Y., Sun, S., 2020. A review of the anti-inflammatory effects of rosmarinic acid on inflammatory diseases. Front. Pharmacol. 11. https://doi.org/10.3389/fphar.2020.00153.

Maheswari, B., Jagadeesh Babu, P.E., Agarwal, M., 2014. Role of N-vinyl-2-pyrrolidinone on the thermoresponsive behavior of PNIPAm hydrogel and its release kinetics using dye and vitamin-B12 as model drug. J. Biomater. Sci. Polym. Ed. 25 (3), 269–286. https://doi.org/10.1080/09205063.2013.854149.

Menduni, F., Davies, L.N., Madrid-Costa, D., Fratini, A., Wolffsohn, J.S., 2018. Characterisation of the porcine eyeball as an in-vitro model for dry eye. Contact Lens and Anterior Eye 41 (1), 13–17. https://doi.org/10.1016/j.clae.2017.09.003.

Meng, M., Chaqour, B., O'Neill, N., Dine, K., Sarabu, N., Ying, G.-S., Shindler, K.S., Ross, A.G., 2024. Comparison of Brn3a and RBPMS labeling to assess retinal ganglion cell loss during aging and in a model of optic neuropathy. Invest. Ophthalmol. Vis. Sci. 65 (4), 19. https://doi.org/10.1167/iovs.65.4.19.

Meschini, S., Pellegrini, E., Maestri, C.A., Condello, M., Bettotti, P., Condello, G., Scarpa, M., 2020. In vitro toxicity assessment of hydrogel patches obtained by cation-induced cross-linking of rod-like cellulose nanocrystals. J. Biomed. Mater. Res. B Appl. Biomater. 108 (3), 687–697. https://doi.org/10.1002/jbm.b.34423.

Mushtaq, N., Schmatz, R., Ahmed, M., Pereira, L.B., da Costa, P., Reichert, K.P., Dalenogare, D., Pelinson, L.P., Vieira, J.M., Stefanello, N., de Oliveira, L.S., Mulinacci, N., Bellumori, M., Morsch, V.M., Schetinger, M.R., 2015. Protective effect of rosmarinic acid against oxidative stress biomarkers in liver and kidney of strepotozotocin-induced diabetic rats. J. Physiol. Biochem. 71 (4), 743–751. https://doi.org/10.1007/s13105-015-0438-4.

Nambiar, M., Schneider, J.P., 2022. Peptide hydrogels for affinity-controlled release of therapeutic cargo: current and potential strategies. J. Pept. Sci. 28 (1). https://doi.org/10.1002/psc.3377.

NIDDK. (2017, May). *Diabetic Eye Disease*. National Institute of Diabetes and Digestive and Kidney Diseases. Retrieved from https://www.niddk.nih.gov/health-information/diabetes/overview/preventing-problems/diabetic-eye-disease.

Pang, W., Wu, J., Zhang, Q., Li, G., 2017. Graphene oxide enhanced, radiation cross-linked, vitamin E stabilized oxidation resistant UHMWPE with high hardness and tensile properties. RSC Adv. 7 (87), 55536–55546. https://doi.org/10.1039/C7RA10637H.

Paradiso, P., Serro, A.P., Saramago, B., Colaço, R., Chauhan, A., 2016. Controlled release of antibiotics from Vitamin E–loaded silicone-hydrogel contact lenses. J. Pharm. Sci. 105 (3), 1164–1172. https://doi.org/10.1016/S0022-3549(15)00193-8.

Peng, C.-C., Kim, J., Chauhan, A., 2010. Extended delivery of hydrophilic drugs from silicone-hydrogel contact lenses containing Vitamin E diffusion barriers. Biomaterials 31 (14), 4032–4047. https://doi.org/10.1016/j.biomaterials.2010.01.113.

Pereira-da-Mota, A.F., Vivero-Lopez, M., Serramito, M., Diaz-Gomez, L., Serro, A.P., Carracedo, G., Huete-Toral, F., Concheiro, A., Alvarez-Lorenzo, C., 2022. Contact lenses for pravastatin delivery to eye segments: design and in vitro-in vivo correlations. J. Control. Release 348, 431–443. https://doi.org/10.1016/j.jconrel.2022.06.001.

Pereira-da-Mota, A.F., Vivero-Lopez, M., Topete, A., Serro, A.P., Concheiro, A., Alvarez-Lorenzo, C., 2021. Atorvastatin-eluting contact lenses: effects of molecular imprinting and sterilization on drug loading and release. Pharmaceutics 13 (5), 606. https://doi.org/10.3390/pharmaceutics13050606.

Pimenta, A.F.R., Valente, A., Pereira, J.M.C., Pereira, J.C.F., Filipe, H.P., Mata, J.L.G., Colaço, R., Saramago, B., Serro, A.P., 2016. Simulation of the hydrodynamic conditions of the eye to better reproduce the drug release from hydrogel contact lenses: experiments and modeling. Drug Deliv. Transl. Res. 6 (6), 755–762. https://doi.org/10.1007/s13346-016-0303-1.

Pollreisz, A., Schmidt-Erfurth, U., 2010. Diabetic cataract—pathogenesis, epidemiology and treatment. J. Ophthalmol. 2010, 1–8. https://doi.org/10.1155/2010/608751.

Potilinski, M.C., Lorenc, V., Perisset, S., Gallo, J.E., 2020. Mechanisms behind retinal ganglion cell loss in diabetes and therapeutic approach. Int. J. Mol. Sci. 21 (7). https://doi.org/10.3390/ijms21072351.

Prausnitz, M.R., Noonan, J.S., 1998. Permeability of cornea, sclera, and conjunctiva: a literature analysis for drug delivery to the eye. J. Pharm. Sci. 87 (12), 1479–1488. https://doi.org/10.1021/js9802594.

Quinn, P. J. (2007). *Molecular Associations of Vitamin E* (pp. 67–98). doi: 10.1016/S0083-6729(07)76004-1.

Ramsay, E., del Amo, E.M., Toropainen, E., Tengvall-Unadike, U., Ranta, V.-P., Urtti, A., Ruponen, M., 2018. Corneal and conjunctival drug permeability: systematic comparison and pharmacokinetic impact in the eye. Eur. J. Pharm. Sci. 119, 83–89. https://doi.org/10.1016/j.ejps.2018.03.034.

Ramsay, E., Lajunen, T., Bhattacharya, M., Reinisalo, M., Rilla, K., Kidron, H., Terasaki, T., Urtti, A., 2023. Selective drug delivery to the retinal cells: Biological barriers and avenues. J. Control. Release 361, 1–19. https://doi.org/10.1016/j.jconrel.2023.07.028.

Serrano, C.A., Villena, G.K., Rodríguez, E.F., 2021. Phytochemical profile and rosmarinic acid purification from two Peruvian Lepechinia Willd. species (Salviinae, Mentheae, Lamiaceae). Sci. Rep. 11 (1), 7260. https://doi.org/10.1038/s41598-021-86692-3.

Shikari, H., Silva, P.S., Sun, J.K., 2014. Complications of intravitreal injections in patients with diabetes. Semin. Ophthalmol. 29 (5–6), 276–289. https://doi.org/10.3109/08820538.2014.962167.

Silva, S.B.da., Costa, J.P., Pintado, M.E., Ferreira, D.de.C., Sarmento, B., 2010. Antioxidants in the prevention and treatment of diabetic retinopathy – a review. Journal of Diabetes & Metabolism 01 (03). https://doi.org/10.4172/2155-6156.1000111.

Silva, P.S., Sun, J.K., Aiello, L.P., 2009. Role of steroids in the management of diabetic macular edema and proliferative diabetic retinopathy. Semin. Ophthalmol. 24 (2), 93–99. https://doi.org/10.1080/08820530902800355.

Simó, R., Sundstrom, J.M., Antonetti, D.A., 2014. Ocular Anti-VEGF therapy for diabetic retinopathy: the role of VEGF in the pathogenesis of diabetic retinopathy. Diabetes Care 37 (4), 893–899. https://doi.org/10.2337/dc13-2002.

Storey, P.P., Obeid, A., Pancholy, M., Goodman, J., Borkar, D., Su, D., Regillo, C., 2020. ocular hypertension after intravitreal injection of 2-MG Triamcinolone. Retina 40 (1), 75–79. https://doi.org/10.1097/IAE.0000000000002361.

Sun, H., Saeedi, P., Karuranga, S., Pinkepank, M., Ogurtsova, K., Duncan, B.B., Stein, C., Basit, A., Chan, J.C.N., Mbanya, J.C., Pavkov, M.E., Ramachandaran, A., Wild, S.H., James, S., Herman, W.H., Zhang, P., Bommer, C., Kuo, S., Boyko, E.J., Magliano, D. J., 2022. IDF Diabetes Atlas: Global, regional and country-level diabetes prevalence estimates for 2021 and projections for 2045. Diabetes Res. Clin. Pract. 183, 109119. https://doi.org/10.1016/j.diabres.2021.109119.

Tang, Y., Shi, Y., Fan, Z., 2023. The mechanism and therapeutic strategies for neovascular glaucoma secondary to diabetic retinopathy. Front. Endocrinol. 14. https://doi.org/10.3389/fendo.2023.1102361.

Tashima, T., 2024. Ocular drug delivery into the eyes using drug-releasing soft contact lens. Future Pharmacology 4 (2), 336–351. https://doi.org/10.3390/futurepharmacol4020019.

Teixeira, J., Lumack do Monte, Z., Tenreiro, S., Salema-Oom, M., Silva, D.C., Saramago, B., Paula Serro, A., 2024. Citicoline eluting hydrogels for therapeutic contact lenses intended to treat neurodegenerative diabetic ocular diseases. Int. J. Pharm. 667, 124908. https://doi.org/10.1016/j.ijpharm.2024.124908.

Toffoletto, N., Salema-Oom, M., Nicoli, S., Pescina, S., González-Fernández, F.M., Pinto, C.A., Saraiva, J.A., Alves de Matos, A.P., Vivero-Lopez, M., Huete-Toral, F., Carracedo, G., Saramago, B., Serro, A.P., 2024. Dexamethasone phosphate and penetratin co-eluting contact lenses: a strategy to enhance ocular drug permeability. Int. J. Pharm. 650, 123685. https://doi.org/10.1016/j.ijpharm.2023.123685.

Toffoletto, N., Saramago, B., Serro, A.P., Chauhan, A., 2023. A physiology-based mathematical model to understand drug delivery from contact lenses to the back of the eye. Pharm. Res. 40 (8), 1939–1951. https://doi.org/10.1007/s11095-023-03560-7.

Tsai, C.-F., Wu, J.-Y., Hsu, Y.-W., 2019. Protective effects of rosmarinic acid against selenite-induced cataract and oxidative damage in rats. Int. J. Med. Sci. 16 (5), 729–740. https://doi.org/10.7150/ijms.32222.

Vazquez, R., Nogueira, R., Orfão, M., Mata, J.L., Saramago, B., 2006. Stability of triglyceride liquid films on hydrophilic and hydrophobic glasses. J. Colloid Interface Sci. 299 (1), 274–282. https://doi.org/10.1016/j.jcis.2006.02.015.

Vieira, L.C., Moreira, C.P.de.S., Castro, B.F.M., Cotta, O.A.L., Silva, L.M., Fulgêncio, G.de. O., Silva-Cunha, A., Fialho, S.L., 2020. Rosmarinic acid intravitreal implants: a new therapeutic approach for ocular neovascularization. Planta Med. 86 (17), 1286–1297. https://doi.org/10.1055/a-1223-2525.

Vivero-Lopez, M., Muras, A., Silva, D., Serro, A.P., Otero, A., Concheiro, A., Alvarez-Lorenzo, C., 2021. Resveratrol-loaded hydrogel contact lenses with antioxidant and antibiofilm performance. Pharmaceutics 13 (4), 532. https://doi.org/10.3390/pharmaceutics13040532.

Wilson, S.L., Ahearne, M., Hopkinson, A., 2015. An overview of current techniques for ocular toxicity testing. Toxicology 327, 32–46. https://doi.org/10.1016/j.tox.2014.11.003.

Wu, Y., Tang, L., Chen, B., 2014. Oxidative stress: implications for the development of diabetic retinopathy and antioxidant therapeutic perspectives. Oxid. Med. Cell. Longev. 2014, 1–12. https://doi.org/10.1155/2014/752387.

Xu, J., Xue, Y., Hu, G., Lin, T., Gou, J., Yin, T., He, H., Zhang, Y., Tang, X., 2018. A comprehensive review on contact lens for ophthalmic drug delivery. J. Control. Release 281, 97–118. https://doi.org/10.1016/j.jconrel.2018.05.020.

Zafar, S., Sachdeva, M., Frankfort, B.J., Channa, R., 2019. Retinal neurodegeneration as an early manifestation of diabetic eye disease and potential neuroprotective therapies. Curr. Diab. Rep. 19 (4), 17. https://doi.org/10.1007/s11892-019-1134-5.

Zhang, X., Zhao, J., Zhao, T., Liu, H., 2015. Effects of intensive glycemic control in ocular complications in patients with type 2 diabetes: a meta-analysis of randomized clinical trials. Endocrine 49 (1), 78–89. https://doi.org/10.1007/s12020-014-0459-8.

Zhou, T., Li, S., Zhu, J., Zeng, G., Lv, Z., Zhang, M., Yao, K., Han, H., 2024. Rosmarinic acid-grafted gelatin nanogels for efficient diquafosol delivery in dry eye disease therapy. J. Control. Release 373, 306–318. https://doi.org/10.1016/j.jconrel.2024.07.026.